

The MgCO_3 – CaCO_3 – Li_2CO_3 – Na_2CO_3 – K_2CO_3 Carbonate Melts: Thermodynamics and Transport Properties by Atomistic Simulations

Elsa Desmaele,^{1, a)} Nicolas Sator,¹ Rodolphe Vuilleumier,² and Bertrand Guillot^{1, b)}

¹⁾ Sorbonne Université, CNRS, Laboratoire de Physique Théorique de la Matière Condensée, LPTMC, F75005, Paris, France

²⁾ PASTEUR, Département de chimie, École normale supérieure, PSL University, Sorbonne Université, CNRS, 75005 Paris, France

Atomistic simulations provide a meaningful way to determine the physico-chemical properties of liquids in a consistent theoretical framework. This approach takes on a particular usefulness for the study of molten carbonates, in a context where thermodynamic and transport data are crucially needed over a large domain of temperatures and pressures (to ascertain the role of these melts in geochemical processes) but are very scarce in the literature, especially for the calco-magnesian compositions prevailing in the Earth's mantle. Following our work on Li_2CO_3 – Na_2CO_3 – K_2CO_3 melts,^{1,2} we extend our force field to incorporate Ca and Mg components. The empirical interaction potentials are benchmarked on the density data available in the experimental literature (for the crystals and the $\text{K}_2\text{Ca}(\text{CO}_3)_2$ melt) and on the liquid structure issued from ab initio molecular dynamics simulations. Molecular dynamics simulations are then performed to study the thermodynamics, the microscopic structure, the diffusion coefficients, the electrical conductivity and the viscosity of molten Ca, Mg-bearing carbonates up to 2073 K and 15 GPa. Additionally, the equation of state of a Na–Ca–K mixture representative of the lavas emitted at Ol Doinyo Lengai (Tanzania) is evaluated. The overall agreement between the MD results and the existing experimental data is very satisfying and provides evidence for the ability of the force field to accurately model any MgCO_3 – CaCO_3 – Li_2CO_3 – Na_2CO_3 – K_2CO_3 melt over a large $T - P$ range. Moreover it is the first report of a force field allowing to study the transport properties of molten magnesite (MgCO_3) and molten dolomite ($\text{CaMg}(\text{CO}_3)_2$).

Keywords: molten carbonates, molecular dynamics, equation of state, microscopic structure, transport properties, diffusion coefficients, electrical conductivity, viscosity, carbonatite

I. INTRODUCTION

Whether it is for the applied or the fundamental fields in which carbonate melts are implied (electrochemistry, geochemistry), having a reliable model for their alkali, alkaline-earth mixtures (and their end-members) is essential. For instance the longevity of molten carbonate fuel cells, usually based on alkali eutectic mixtures, is known to be improved by the addition of alkaline-earth cations,³ in a small enough amount that doesn't compromise the efficiency of the cell.^{3–7} From the viewpoint of geosciences, carbonate melts, although they constitute a very minor phase of the Earth's mantle (the most part is silicate), are thought to have important implications in the lowering of the melting temperature of silicate rocks, the deep carbon cycle or the high conductivity anomalies observed in the 70–200 km depth region.^{8–12} On Earth, evidence of a past volcanic activity induced by carbonatitic lava ($\text{SiO}_2 < 20$ wt%) is given by petrology.^{13,14} Nowadays, Ol Doinyo Lengai in Tanzania is the only active volcano to produce these remarkable (low temperature, low viscosity) carbonatitic lavas. The carbonatitic melt is mainly composed of a Na_2CO_3 – K_2CO_3 – CaCO_3 mixture (in proportions 55:9:36 mol% according to Keller and Zaitsev¹⁵), called natrocarbon-

atite, whereas the majority of other inventoried carbonatites are of calco-magnesian composition.¹⁶ In addition, in the Earth's mantle the most abundant carbonate compositions are calcite, CaCO_3 , predominating at shallow depth and magnesite, MgCO_3 , progressively taking over as depth increases. As a consequence their mixture and particularly dolomite, $\text{CaMg}(\text{CO}_3)_2$, are of major interest. For pressure of a few kbars and beyond, these Ca,Mg-carbonates form stable liquid phases over a wide temperature domain.^{17–19} But at atmospheric pressure they break down into CO_2 + oxide (CaO , MgO) at temperatures below their melting point (decarbonation occurs for P below ~ 1 GPa for calcite and ~ 3 GPa for magnesite and dolomite).^{20,21} Consequently only a few data are available in the literature for calco-magnesian compositions (most of which are alkali-bearing mixtures stable at low pressure),^{3,9,22} and very few at high pressures.^{23–25} Thus for molten MgCO_3 there is simply no data to our knowledge.²⁶

In this context where experimental data are sparse in terms of thermodynamic conditions, chemical composition and physical properties, a noticeable advantage of molecular dynamics simulations (classical and ab initio) is that a variety of properties (structure, equation of state and transport coefficients) can be computed in the same theoretical framework. However, one has to be aware that collective quantities such as the ionic conductivity and the viscosity are calculated from slowly converging time correlation functions, that necessarily require (to be accurate) a rather large number of atoms and long time

^{a)} Electronic mail: elsa.desmaele@gmail.com

^{b)} Electronic mail: guillot@lptmc.jussieu.fr

runs. For this reason, *ab initio* molecular dynamics simulations (AIMD), deriving from electronic density calculations, are either restricted to the study of thermodynamics and structure properties^{27,28} or only provide crude estimates of transport coefficients, especially when it is question to establish their evolution with pressure and temperature.^{29,30} As for classical molecular dynamics simulations (MD), based on a more empirical approach, very few studies have provided estimates of the viscosity and electrical conductivity of carbonate melts, namely CaCO_3 ,²⁹ the Li_2CO_3 - K_2CO_3 eutectic mixture (62:38 mol%)³¹ and more recently the Li_2CO_3 - Na_2CO_3 - K_2CO_3 mixtures and end-members.¹ Obviously, the scarcity of thermodynamic data^{26,32,33} does not help for developing empirical potentials. As a consequence, very few force fields (FF) are available for Ca-Mg and most of them were developed for crystals³⁴⁻⁴⁰ based on the Born model of solids.⁴¹ A first step towards an accurate description of the CaCO_3 melt was made by Genge *et al.*⁴² by adapting the FF of Dove *et al.*³⁵ (for the crystal). The resulting FF reproduces quite well the liquid structure issued from a AIMD calculation published long after,²⁹ but the calculated pressure is overestimated by $\sim +15$ kbar, compared to the recently published equation of state of Zhang and Liu²⁷ based on AIMD calculations. Moreover the melting temperature is underestimated. Both these features point toward a too weakly cohesive melt, that may result from the absence of dispersion interaction in the FF.¹ In another attempt Hurt and Wolf⁴³ adapted the model of Archer *et al.*³⁹ and proposed a FF fitted on crystalline properties for carbonates in the CaCO_3 - SrCO_3 - BaCO_3 system.

For MgCO_3 , in absence of experimental data, Hurt and Wolf⁴³ only list in their study some FF parameters, but no explanation on the way they were derived and no result is given for this composition. In the present study, we have developed an empirical force field to describe the thermodynamics and transport properties of MgCO_3 - CaCO_3 melts.

In a previous study devoted to the Li_2CO_3 - Na_2CO_3 - K_2CO_3 system, we have demonstrated the ability of molecular dynamics (MD) simulations to reproduce experimental data for alkali carbonate melts.¹ Here we extend the latter study to incorporate alkaline-earth components (Mg, Ca). In our study of alkali carbonates we evidenced the need to take into account in the FF the dispersion interactions, which were not included in the FF previously developed by our team for CaCO_3 .²⁹ Thus for the sake of consistency the interactions between the carbonate anions and the alkali or alkaline-earth cations are treated on the same footing in the present FF. In section II the details of the simulations are presented. In section III the thermodynamic properties (equation of state) and the liquid structure are reported, whereas in section IV we evaluate the transport coefficients (diffusion coefficients, electrical conductivity and viscosity). Furthermore, the heuristic of the Nernst-Einstein equation (relating the electrical conductivity and diffusion co-

efficients) and of the Stokes-Einstein equation (relating the viscosity and diffusion coefficients) is evaluated and commented.

II. METHOD

A. Computational details

1. *Ab initio* molecular dynamics (AIMD)

Two AIMD simulations were run for this study, one for molten magnesite (MgCO_3) and one for molten dolomite ($\text{CaMg}(\text{CO}_3)_2$). They were based on the density functional theory (DFT) within the Born-Oppenheimer approximation using the freely available QUICKSTEP/CP2K software⁴⁴ that applies a hybrid Gaussian/plane-wave method.⁴⁵ For the study of $\text{CaMg}(\text{CO}_3)_2$ we used for the valence electrons of carbon and oxygen a triple- zeta valence plus polarization basis set optimized for molecules (TZV2P).⁴⁶ Otherwise we used a double-zeta plus polarization basis set (DZVP).⁴⁷ Core electrons were treated by the Goedecker-Teter-Hutter (GTH) norm conserving pseudo-potentials.⁴⁸⁻⁵⁰ The cutoff for the electronic density was set to 700 Ry. Exchange and correlation interactions were accounted for by the gradient corrected BLYP functional^{51,52} using a semi-empirical D3 dispersion correction scheme with a cutoff $\geq \sqrt{3}L$, where L is the length of the simulation box.⁵³ All DFT calculations were run in the *NVT* ensemble with the temperature set constant by a Nosé-Hoover thermostat.^{54,55}

For MgCO_3 and for $\text{CaMg}(\text{CO}_3)_2$ the simulations were run with 200 atoms for 20 ps and with 640 atoms for 12 ps at state points (1873 K, 2.49 g/cm³) and (1773 K, 2.25 g/cm³), leading to an average pressure of 4.5 ± 1.5 and 1.8 ± 1.0 GPa, respectively. For information, congruent melting is known to occur at 2.7 GPa and 1850 K for magnesite²⁰ and at 2.7 GPa and 1653 K for dolomite.²⁰ As for molten calcite (CaCO_3), the AIMD simulations of Vuilleumier *et al.*²⁹, based on the same DFT approach, were used as benchmark.

B. Classical molecular dynamics (MD)

Classical MD simulations were carried out using the DL-POLY 2 software,⁵⁶ with a timestep of 1 fs. Density calculations were performed in the *NPT* ensemble with a Nosé-Hoover thermostat for a simulation time of $t \simeq 0.9$ ns (including a 0.5 ns equilibration run) allowing to reach an accuracy on the density value of $\Delta n/n \sim \pm 1\%$. To evaluate the transport coefficients, simulations were performed in the *NVE* ensemble with an equilibration run of 0.5 ns, followed by a production run of 10 to 30 ns. Structural data were extracted from the same simulations. All simulations had a system size $N \simeq 2000$

i	j	A_{ij} (kJ/mol)	ρ_{ij} (Å)	C_{ij} (Å ⁶ /mol)	q_i (e)
Mg	O	243 000	0.24335	1 439	+1.64202
Ca	O	200 000	0.2935	5 000	+1.64202
Li	O	300 000	0.2228	1 210	+0.82101
Na	O	1 100 000	0.2228	3 000	+0.82101
K	O	900 000	0.2570	7 000	+0.82101
O	O	500 000	0.252525	2 300	-0.89429

TABLE I: Intermolecular Buckingham parameters and partial charges. Note that for electroneutrality considerations $q_C = +1.04085$ e. Intramolecular Born repulsion parameters between oxygen atoms of a same carbonate ion are $A_{OO}^{intra-CO_3} = 2611707.2$ kJ/mol and $\rho_{OO}^{intra-CO_3} = 0.22$ Å.

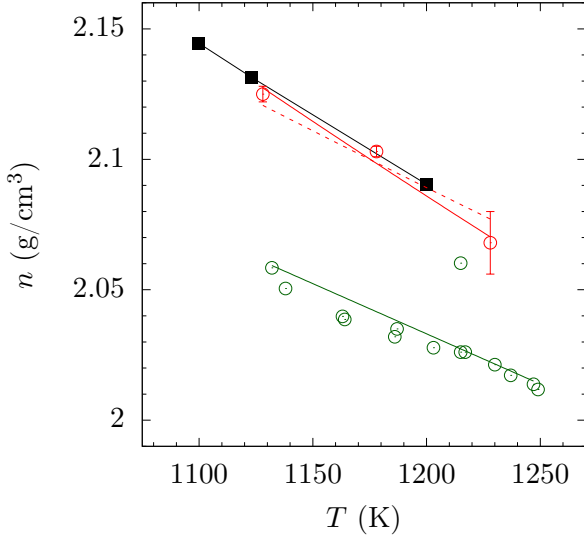


FIG. 1: Density of the molten $K_2Ca(CO_3)_2$ mixture from MD simulations (squares) and from experimental measurements (circles) of Liu and Lange³² (red) and Dobson *et al.*²³ (green). The lines correspond to a linear fit. The dotted line is the extrapolation of Liu and Lange³² using an ideal mixing rule.

atoms, except for specific calculations that used the number of atoms as the AIMD simulations in order to compare at best the pair distribution functions obtained by both approaches.

C. Force Field

The force field is composed of interionic pair potentials as presented in a previous paper.¹ The intramolecular part (interactions within a carbonate molecule) contains an oxygen-oxygen term: $V_{OO}^{intra-CO_3}(r_{OO}) = A_{OO}^{intra-CO_3} \exp(-r_{OO}/\rho_{OO}^{intra-CO_3})$, and a carbon-oxygen term: $V_{CO}^{intra-CO_3}(r_{CO}) =$

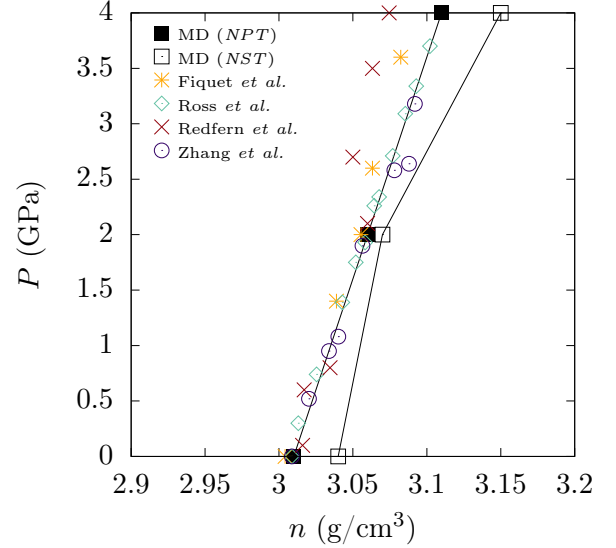


FIG. 2: Density-pressure diagram for crystalline magnesite $MgCO_3$ at 300 K from the experimental literature (colored symbols)^{57–60} and obtained from MD calculations in the NPT ensemble (filled black squares and black line as a guide to the eye) and in the NST ensemble (empty black squares and black line as a guide to the eye).

$k_{CO}(r_{CO} - r_{0,CO})^2/2 + q_O q_C / 4\pi\epsilon_0 r_{CO}$, with a force constant $k_{CO} = 6118.17$ kJ/mol and an harmonic equilibrium distance $r_{0,CO} = 1.30$ Å adjusted so as to obtain a mean C–O distance of 1.29 Å, as found by X-ray diffraction measurements and AIMD simulations.^{1,29,62} Two ions i and j , with $i, j = Li, Na, K, Ca, Mg, O$ and C (with O and C not belonging to a same carbonate group) interact through the following intermolecular potential: $V_{ij}^{inter}(r_{ij}) = A_{ij} \exp(-r_{ij}/\rho_{ij}) - C_{ij}/r_{ij}^6 + q_i q_j / 4\pi\epsilon_0 r_{ij}$. Table I recaps the previously published parameters for the Li–Na–K melts,¹ and provides the parameters for Mg and Ca. The latter parameters were adjusted so as to reproduce at best (i) the density measurements of crystalline $MgCO_3$, $CaCO_3$ and $CaMg(CO_3)_2$ at 300 K and 1 bar, the density and the compressibility of the K_2CO_3 – $CaCO_3$ melt at 1 bar and 1100–1200 K, and (ii) the microscopic structure, in the form of atomic pair distribution functions (PDFs), issued from AIMD simulations of the $CaCO_3$, $MgCO_3$ and $CaMg(CO_3)_2$ melts.

At variance with alkali carbonates, alkaline-earth carbonates do not form stable melts under atmospheric pressure^{17,20,21,63,64} and no reliable measurement of their density under high pressure has been published yet. However molten calcium carbonate is stable at 1 bar in mixtures with alkalis. In particular, the density of the equimolar K_2CO_3 – $CaCO_3$ mixture has been measured by Liu and Lange³² using an advanced double-bob Archimedean method overcoming artifacts

	MgCO ₃	CaCO ₃	CaMg(CO ₃) ₂	K ₂ Ca(CO ₃) ₂	Natro
n_{MD}^0 (g/cm ³)	2.49	2.44 (2.47 [†] , 2.44 [‡])	2.49	2.14	2.11
$n_{MD,mix}^0$ (g/cm ³)	–	–	2.46	2.12	2.11
$n_{Exp,mix}^0$ (g/cm ³)	2.45	2.49	2.47	2.13	2.13
K_{MD}^0 (GPa)	15.0	17.6 (15.7 [†] , 15.1 [‡])	12.8	9.1	11.4
$K_{MD,mix}^0$ (GPa)	–	–	–	8.6	10.4
$K_{Exp,mix}^0$ (GPa)	–	18.7	–	8.9	10.4

TABLE II: Density and bulk modulus of MgCO₃, CaCO₃ and CaCO₃-bearing mixtures at $T = 1100$ K calculated either by MD simulations (n_{MD}^0 , K_{MD}^0) or by using ideal mixing rules ($n_{MD,mix}^0$, $K_{MD,mix}^0$). Extrapolation from experiments $n_{Exp,mix}^0$, $K_{Exp,mix}^0$ are given for comparison.^{32,61} Note that for MgCO₃ an additional assumption relative to the cationic mass is needed to estimate $n_{Exp,mix}^0$ (see Hurt and Lange²⁶). In parenthesis are given the MD results from the models of Vuilleumier *et al.*²⁹ ([†]) and Hurt and Wolf⁴³ ([‡]).

due to surface tension and to the mass of the bob, and which reproduced with a great accuracy the density of many liquid standards.⁶⁵ As shown on Fig. 1 the agreement between the density measurements of Liu and Lange³² on the K–Ca melt and our MD calculation is excellent. Note that Dobson *et al.*²³ also measured the density of this mixture but the values they report are by $\sim 5\%$ lower than the ones from Liu and Lange.³² Additionally, Liu and Lange³² have suggested that the density of molten carbonates virtually has an ideal behavior regarding composition:^{1,32}

$$n_{mix} = \frac{\sum_i x_i M_i}{\sum_i x_i \bar{V}_i}, \quad (1)$$

where x_i is the molar fraction of species i of molar mass M_i and molar volume \bar{V}_i . Although this approximation is fairly good for purely alkali mixtures, it seems less accurate for mixtures containing both alkali and alkaline-earth cations (see Fig. 1 and next section). Still this mixing rule allows to extrapolate the density of an hypothetical CaCO₃ liquid at 1 bar.³² In a MD simulation such a liquid is metastable, meaning that it is possible to evaluate its density straightforwardly, at variance with the experiments. Satisfactorily the density calculated by MD (e.g. 2.44 g/cm³ at 1100 K) is fairly compatible with the extrapolation proposed by Liu and Lange³² (2.49 g/cm³ at 1100 K).

For MgCO₃ no measurement of density, not even in a mixture, has been published yet. But based on the density of various carbonates (in the Li₂CO₃–Na₂CO₃–K₂CO₃–Rb₂CO₃–Cs₂CO₃–CaCO₃–SrCO₃–BaCO₃ system) and considering how this property evolve as a function of the cationic radius, Hurt and Lange²⁶ suggested that an hypothetical MgCO₃ melt at 1 bar and 1100 K would have a density of 2.45 g/cm³. This guess is within 2% of the density we obtained by simulating the metastable liquid (2.49 g/cm³). So by introducing in Eq. (1) the density of molten calcite (from Liu and Lange³²) and that of magnesite (from Hurt and Lange²⁶) at the chosen reference state of 1 bar and 1100 K gives a density of 2.47 g/cm³ for the CaMg(CO₃)₂ melt, in close match with the value of 2.49 g/cm³ as ob-

tained by MD (Table II).

As the densities of molten magnesite and calcite proposed by Hurt and Lange²⁶ are merely an approximate estimation, we chose to test the accuracy of our FF by calculating the density of the crystalline phases that are well constrained even under high $T - P$.^{57–60,66} We chose to focus on the calcite structure (rhombohedral) as it is a common polymorph to MgCO₃, CaCO₃ and CaMg(CO₃)₂.⁶⁷ For magnesite at 300 K up to 4 GPa (Fig. 2), the calculated density is in excellent agreement with the experimental values, well within the scattered data of the experimental literature. Moreover MD simulations reproduce very well the compressibility: $K_T = 125$ GPa as compared to 117 GPa according to Ross.⁶⁰ We believe this should lead to a reliable evaluation of densities for the liquid phase. We also calculated the density of calcite (CaCO₃) at room conditions and obtained 2.63 g/cm³, against 2.71 and 2.72 g/cm³ according to Redfern *et al.*⁵⁷ and Fiquet *et al.*,⁵⁸ respectively, that is within $\sim 3\%$. For comparison, at the same conditions AIMD yielded 2.67 g/cm³.²⁹ For dolomite, the agreement between MD ($n = 2.81$ g/cm³) and the X-ray diffraction data ($n = 2.84$ g/cm³)⁵⁸ is even better with a deviation of -1% . The densities were also calculated by anisotropic relaxation of the crystal structure (MD simulations in the *NST* ensemble). The accuracy of the MD-calculated values deteriorates slightly for magnesite ($n = 3.04$ g/cm³ instead of 3.01, see Fig. 2) but improves for dolomite ($n = 2.84$ g/cm³) and remains unchanged for calcite. Tables S1 and S2 in the supplementary material detail the lattice parameters and the calculated density values up to 4 GPa.

III. THERMODYNAMICS

A. Equation of State

Although there exist no measured data of the density of calco-magnesian carbonate melts, an estimation can be made by assuming that carbonate liquids mix linearly with respect to carbonate components (ideal mix-

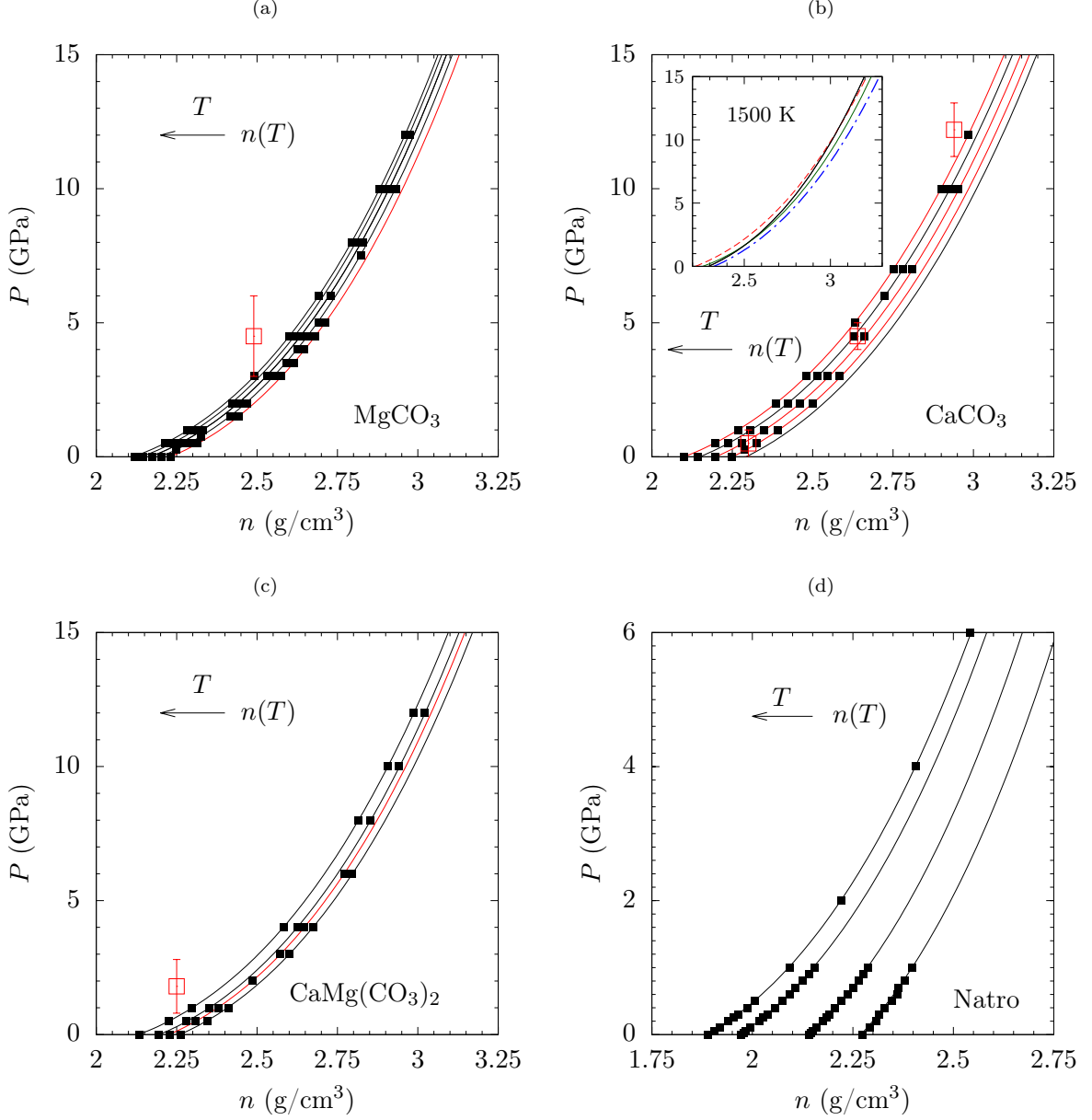


FIG. 3: MD (black) and AIMD (red) calculated density-pressure points. Compression isotherms (black or red curves) are interpolated from the MD points by the Birch-Murnaghan equation of state (BMEoS). The temperature of the MD isotherms are: {1873 K, 1973 K, 2073 K, 2173 K, 2273 K} for MgCO_3 (a), {1500 K, 1623 K, 1773 K, 1923 K, 2073 K} for CaCO_3 (b), {1653 K, 1773 K, 1873 K, 2073 K} for $\text{CaMg}(\text{CO}_3)_2$ (c) and {823 K, 1073 K, 1423 K, 1600 K} for the natrocarbonatite (Natro) $\text{Na}_{1.1}\text{K}_{0.18}\text{Ca}_{0.36}\text{CO}_3$ (d). Red squares are AIMD points: 1873 K for MgCO_3 , 1623 K, 1773 K and 2073 K for CaCO_3 and 1773 K for $\text{CaMg}(\text{CO}_3)_2$. The compression curves at the corresponding temperatures are plotted in red to facilitate the comparison between MD and AIMD results.

For CaCO_3 a BMEoS isotherm issued from the experimental thermodynamics data and fusion curve analysis at 1500 K is also plotted in the inset (dashed dotted blue curve)^{32,61,68} along with the isotherms calculated from AIMD by Zhang and Liu²⁷ (dashed red curve) and from MD by Vuilleumier *et al.*²⁹ (green) at the same temperature (the present study is the black curve).

ing assumption). As discussed above, this allowed Liu and Lange³² to estimate the density of molten CaCO_3 at 1-bar. Now, to infer the high pressure properties of these liquids, constraining the 1-bar compressibility is also needed. Then the density of molten carbonates can be accurately modeled by the third-order Birch Murnaghan equation of state (BMEoS):⁶⁹

$$P = \frac{3}{2}K^0(T) \left(\left(\frac{n}{n_T^0} \right)^{7/3} - \left(\frac{n}{n_T^0} \right)^{5/3} \right) \times \left(1 - \frac{3}{4}(4 - K'^0) \left(\left(\frac{n}{n_T^0} \right)^{2/3} - 1 \right) \right), \quad (2)$$

where n_T^0 is the atmospheric density at temperature T , K_T^0 the bulk modulus (inverse of the compressibility) and K'^0 its pressure derivative at 1 bar (note that it is a constant under the thermodynamic conditions of this study). After fitting our MD data, we propose an equation of state for MgCO_3 , $\text{CaMg}(\text{CO}_3)_2$ and for a natrocarbonatite ($\text{Na}_{1.10}\text{K}_{0.18}\text{Ca}_{0.36}\text{CO}_3$) modeling the carbonatitic lavas from Ol Doinyo Lengai (see Table III). O'Leary *et al.*⁶¹ measured the compressibility of the alkali end-members and several mixtures of the system CaCO_3 – Na_2CO_3 – K_2CO_3 – Li_2CO_3 , including mixtures containing various ratios of CaCO_3 . Then they extrapolated the 1 bar compressibility of molten CaCO_3 , that is a metastable liquid at this pressure, by using an ideal mixing rule:

$$K_{mix} = \frac{\sum_i x_i \bar{V}_i}{\sum_i x_i \bar{V}_i / K_i}. \quad (3)$$

The comparison of our MD results with their study is good as shown in Table II. In particular our results are in a better agreement than when using the FFs developed by Vuilleumier *et al.*²⁹ and by Hurt and Wolf.⁴³ Then O'Leary *et al.*⁶⁸ used fusion curve analysis to constrain $K'^0 = 7 \pm 1$, still for CaCO_3 . Note that this value is closer to the one produced using our FF ($K'^0 = 8.2$, as in²⁹) than using the one of Hurt and Wolf⁴³ ($K'^0 = 10.3$). Inserting this value, as well as the 1-bar density from Liu and Lange³² and the 1-bar compressibility from O'Leary *et al.*⁶⁸ in Eq. (2) we built an experimental compression curve for CaCO_3 at 1500 K (see the inset in Fig. 3b). This estimation is very close to the one issued from our MD simulations.

Based on AIMD simulations, Zhang and Liu²⁷ proposed an equation of state for CaCO_3 . However, because of the LDA approximation they used to compute exchange-correlation energies, an approximation which tends to overestimate the density (at a given P), the authors have applied a rescaling method. The compression curve given by their equation of state at 1500 K is plotted in the inset of Fig. 3b for CaCO_3 . It fits our MD compression curve quite well although there remains a slight deviation at low pressure. Moreover, the compressibility provided by our model is slightly lower than the one from

Zhang and Liu²⁷. However that may be, at 1500 K, we get $K_{1500\text{K}}^0 = 13.7$ GPa, just like O'Leary *et al.*,⁶¹ whereas Zhang and Liu²⁷ give a value of 11.9 GPa. As for the AIMD calculations we performed (this study and Vuilleumier *et al.*²⁹), they are based on the GGA approximation and include a (semi-empirical) correction for dispersion forces. The introduction of dispersion interactions enhances interionic cohesion in the liquid, but maybe not sufficiently, a feature which could account for the slight remaining difference between MD and AIMD ($P_{MD} < P_{AIMD}$ in general, see Fig. 3).

If the number density, ρ , is considered (rather than mass density n), it goes as follow at 3 GPa and 1873 K: $\rho_{\text{MgCO}_3} = 40.1$ mol/L $>$ $\rho_{\text{CaCO}_3} = 25.2$ mol/L, which is consistent with the observation made for alkali melts,¹ that the number density is negatively correlated to the cation size. However, the bulk modulus is the same in magnesite and calcite ($K_{\text{MgCO}_3}^0 = K_{\text{CaCO}_3}^0 = 11.0$ GPa), at variance with alkali melts where K^0 increases with increasing cation radius. This suggests that the compressibility of calco-magnesian carbonate melts is not similar to that of a hard sphere system and instead is dominated by the coulombic repulsion between divalent cations. If we consider the compressibility at 1 bar and 1100 K of the metastable MgCO_3 and CaCO_3 melts ($K_{\text{MgCO}_3}^0 = 14.0$ GPa and $K_{\text{CaCO}_3}^0 = 17.6$ GPa), it is greater by a factor ~ 2 than that of alkali carbonates at the same $T - P$ conditions. However, the compressibilities calculated in corresponding states (i.e. near the melting point, 1823 K and 3 GPa for MgCO_3 , and 1623 K and 1 GPa for CaCO_3) are very similar ($K_{1823\text{K}}^{3\text{GPa}} = 7.5$ GPa for MgCO_3 and $K_{1623\text{K}}^{1\text{GPa}} = 6.4$ GPa for CaCO_3) for both alkali and alkaline-earth carbonates.

Knowing the equations of state for MgCO_3 , CaCO_3 , Na_2CO_3 , K_2CO_3 and Li_2CO_3 and some mixtures (dolomite and natrocarbonatite) it is worth checking how these latter melts behave regarding ideality (Table II). For that we consider, for instance, the density of molten dolomite at 1 bar and at 3 GPa, let's say at 1873 K. The comparison between the raw MD data and the ideal mixing rules (Eqs. (1) and (3)) using the data of Table III gives: $n_T^0 = n_T^{0,mix} = 2.19$ g/cm³ and $K_T^0 = K_T^{0,mix} = 11.0$ GPa, and $n_T^{3\text{GPa}} = n_T^{3\text{GPa},mix} = 2.55$ g/cm³. Proceeding the same way for the natrocarbonatite at 1 bar and 1073 K we get $n_T^0 = 2.11$ g/cm³ and $n_T^{0,mix} = 2.13$ g/cm³, and $K_T^0 = 11.4$ GPa and $K_T^{0,mix} = 10.4$ GPa. Hence it comes out that dolomite is an ideal mixture on a certain P -domain, whereas natrocarbonatite slightly deviates from ideality. Most likely the latter finding can be explained by the fact that the natrocarbonatite includes both uni- and divalent cations. In practice, as the deviation from ideality seems to be fairly small, the EoS of the end-members of the Mg–Ca–Li–Na–K system can be used to estimate with confidence the density of any mixture.

	MgCO ₃	CaCO ₃	CaMg(CO ₃) ₂	Natro
T (K)	1873 – 2073	1100 – 2073	1653 – 2073	823 – 1600
P (GPa)	0 – 15	0 – 15	0 – 15	0 – 6
T_{ref} (K)	1873	1623	1653	1073
n_{ref} (g/cm ³)	2.23	2.25	2.26	2.14
α_0 (K ⁻¹)	-1.50×10^{-4}	-1.54×10^{-4}	-1.23×10^{-4}	-2.36×10^{-4}
α_1 (K ⁻²)	8.22×10^{-8}	0.49×10^{-8}	-7.65×10^{-8}	-0.20×10^{-8}
K_{ref}^0 (GPa)	10.98	12.74	12.13	11.72
b_1 (K ⁻¹)	5.0×10^{-4}	6.1×10^{-4}	3.7×10^{-4}	10.2×10^{-4}
b_2 (K ⁻²)	2.0×10^{-7}	1.5×10^{-7}	5.0×10^{-7}	7.7×10^{-7}
K^{70}	8.5	8.2	8.5	8.0

TABLE III: Parameters of the third-order Birch-Murnaghan equation of state and $T - P$ domain of validity. Natro refers to the natrocarbonatite melt of composition $\text{Na}_{1.1}\text{K}_{0.18}\text{Ca}_{0.36}\text{CO}_3$ (see text).

The reference temperature T_{ref} is defined for numerical purposes and set to the melting temperature for each composition, n_{ref}^0 and K_{ref}^0 are the density and bulk modulus at 1-bar and T_{ref} . Other empirical parameters (α_0 , α_1 , b_1 and b_2) are defined by $n_T^0 = n_{ref}^0 e^{\int_{T_{ref}}^T -(\alpha_0 + \alpha_1 T) dT}$ and $K_T^0 = K_{ref}^0 / (1 + b_1(T - T_{ref}) + b_2(T - T_{ref})^2)$. See Desmaele *et al.*¹ for details on the fitting method.

B. Structure

In the $T - P$ range of this study ($T \leq 2013$ K and $P \leq 15$ GPa), the stability of the internal structure of the carbonate ion has been pointed out by neutron diffraction measurements,⁷⁰ *in situ* X-ray diffraction measurements³³ and by AIMD simulations (Ref. 1 and 29 and this study). Moreover the carbonate anion, unlike the SiO_4 units in silicates, cannot share a covalent bond with other atoms. Therefore carbonate melts display a structure contrasting with that of most geological melts (silicate) that are always polymerized to a certain degree. This is why carbonate melts share with molten salts (e.g. NaCl) a high ionic diffusivity and a low viscosity. Until now, among the alkaline-earth carbonates, only the structure of calcite melt has been investigated by classical molecular dynamics simulations^{29,42,43} and by AIMD simulations.^{29,30} Fig. 4 shows the PDFs for MgCO_3 and CaCO_3 at corresponding states (i.e. near melting point: $T = 1873$ K, $P \sim 2$ GPa and $n = 2.49$ g/cm³ for MgCO_3 ; $T = 1623$ K, $P \sim 0.5$ GPa and $n = 2.30$ g/cm³ for CaCO_3). Note that, as expected, they are in very good agreement with the PDFs issued from AIMD (compare the plain lines with the dotted lines). The first peak of $g_{\text{CO}}(r)$ at $r_{\text{CO}} = 1.29$ Å corresponds to the three oxygen atoms bonded to a same carbon atom in a carbonate unit. Between 1.7 Å and 2.1 Å $g_{\text{CO}}(r) = 0$ because no C–O bond dissociation occurs during the simulation. On the other hand, the first peak of g_{OO} represents the O–O intramolecular distance ($r_{\text{OO}} = 2.22$ Å) in a carbonate ion. The first minimum of g_{OO} is non-zero, meaning that the distance between two oxygen atoms of two different CO_3^{2-} units may be as short as the O–O intramolecular distance. Concerning the anion-anion correlations, each CO_3^{2-} unit is surrounded by 12 – 15 other carbonate ions at $r_{\text{CC}} \simeq 4 - 6$ Å on average. The first C–C peak on Fig. 4a is broad with a shouldering on its low- r flank

(3.5 – 4 Å), that is especially noticeable for MgCO_3 , and a small bump at $\sim 5 - 7$ Å in the region of the first minimum, this time more pronounced in CaCO_3 . Each cation (Mg^{2+} or Ca^{2+}) ion is surrounded by 6 carbonate groups (against 4.5 – 4.8 for alkali), at a mean cation-carbon distance of 3 – 4 Å in MgCO_3 and 3.15 – 4.5 Å in CaCO_3 (note that these distances are the same in $\text{CaMg}(\text{CO}_3)_2$ at 1773 K and 2.25 g/cm³). As for the ratio of the coordination numbers $N_c^{\text{X-O}}/N_c^{\text{X-C}}$ (where X = Mg or Ca), indicative of the orientation of the carbonate ions around the cations, it is 1.1 for Mg and 1.3 for Ca (as compared to 1.3 – 1.6 for alkali cations). In comparison to pair distribution functions for alkali carbonate melts, the cation-anion PDF $g_{\text{XC}}(r)$ for alkaline-earth carbonates are more simple as they show no shoulder on the first peak (see Fig.4b and compare with Fig. 2 in Desmaele *et al.*¹). Moreover, the second peak of $g_{\text{XC}}(r)$ is broader, especially for Mg. It can also be noted that the shape of the PDFs is less sensitive to the size of the cation. Looking at the cation-cation PDFs, the only difference between Mg and Ca is the amplitude, greater for the Ca–Ca pair with a coordination number around ~ 10 instead of ~ 7 for Mg–Mg. It is noteworthy that the PDFs of $\text{CaMg}(\text{CO}_3)_2$ are intermediate between those of CaCO_3 and MgCO_3 . In fact, most structural features observed in molten calcite and magnesite are similar and can be interpreted as a simple homothetic transformation upon volumetric change from CaCO_3 to MgCO_3 . Thus the pair distribution functions X–C, X–O and X–X in $\text{CaMg}(\text{CO}_3)_2$ are almost identical to the corresponding ones observed in CaCO_3 and MgCO_3 (Fig. 4b) and this remains true even at high pressures (Figs. S1, S2 and S3 in the supplementary material). Under pressure (and up to 12 GPa), the PDFs shift progressively towards lower distances, reflecting the melt compaction (see Figs. S1, S2 and S3). Moreover the average number of CO_3^{2-} anions around cations increases slightly under pressure,

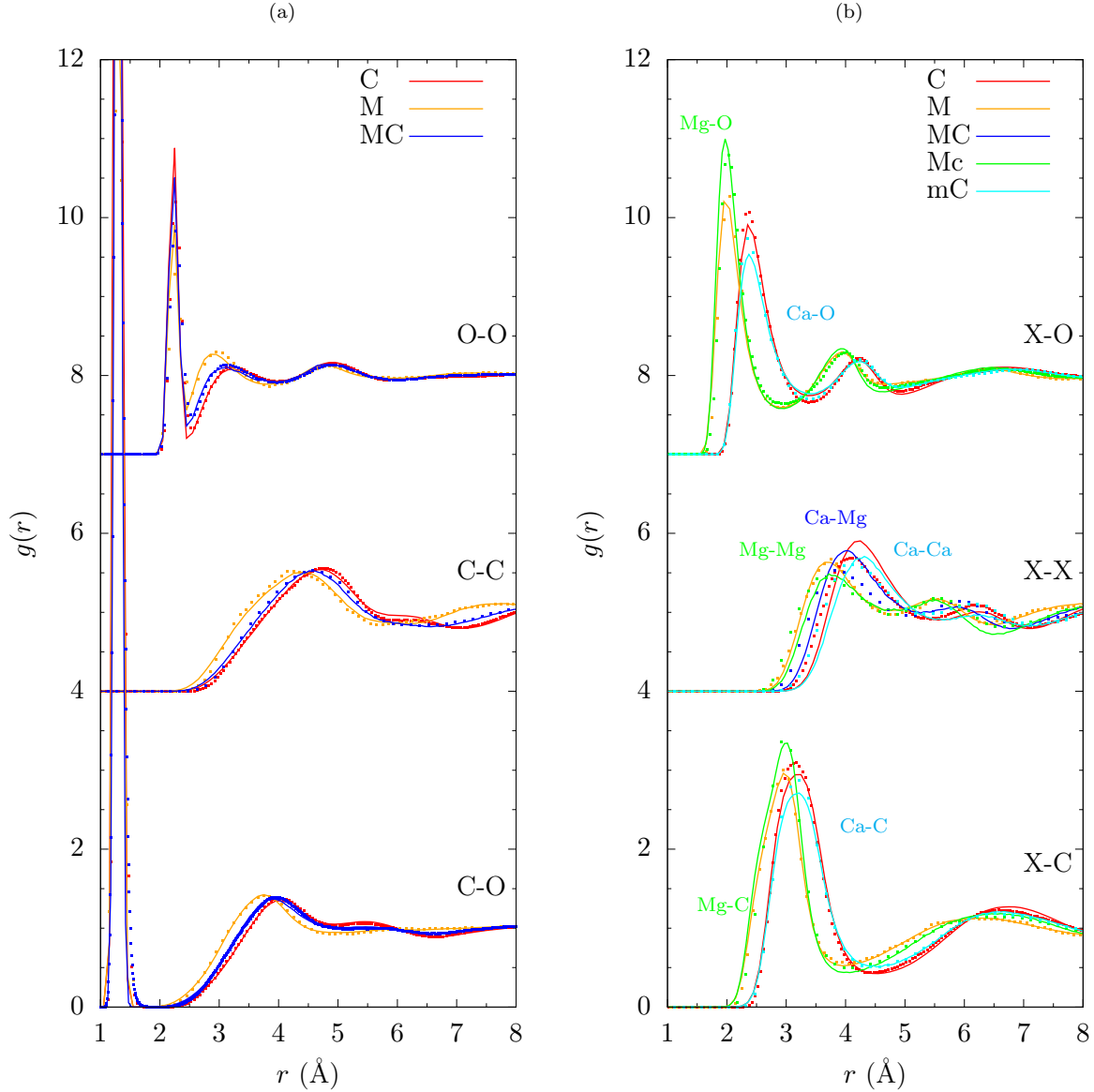


FIG. 4: MD pair distribution functions O–O, C–C, C–O, X–O, X–X and X–C where C and O are carbon and oxygen atoms of the CO_3^{2-} ions and $\text{X}=\text{Ca}$ or Mg (see color code) in MgCO_3 (M) at 1873 K and 2.49 g/cm^3 , CaCO_3 (C) at 1623 K and 2.30 g/cm^3 and $\text{CaMg}(\text{CO}_3)_2$ (MC) at 1773 K and 2.25 g/cm^3 . The labels "Mc" and "mC" refer to the MgCO_3 and to the CaCO_3 components of $\text{CaMg}(\text{CO}_3)_2$, respectively. The PDFs calculated from the AIMD simulations (this study and Ref.²⁹) at the same temperature and density are represented by the dotted lines (plain lines for MD). To facilitate visualization, the different PDFs were shifted vertically.

from 6 to 7. In contrast, the coordination number of CO_3^{2-} around CO_3^{2-} ($\sim 12 - 15$) does not evolve with pressure, neither does the $N_c^{\text{X-O}}/N_c^{\text{X-C}}$ ratio.

IV. TRANSPORT PROPERTIES

For MgCO_3 , CaCO_3 and $\text{CaMg}(\text{CO}_3)_2$, a series of simulations (~ 15) was performed at different thermody-

namic conditions, with a duration long enough to reach the diffusive regime (10 – 20 ns). From each run we calculated accurately (see below) the self-diffusion coefficients D_s of each chemical species $s = \text{Ca}$, Mg and CO_3^{2-} , the electrical conductivity σ and the viscosity η ,

given by:^{71,72}

$$D_s = \lim_{t \rightarrow \infty} \frac{1}{6t} \frac{1}{N_s} \sum_{i=1}^{N_s} \left\langle |\mathbf{r}_i(t) - \mathbf{r}_i(0)|^2 \right\rangle, \quad (4)$$

$$\sigma = \lim_{t \rightarrow \infty} \frac{1}{6t} \frac{e^2}{k_B T V} \left\langle \left| \sum_{i=1}^N z_i (\mathbf{r}_i(t) - \mathbf{r}_i(0)) \right|^2 \right\rangle, \quad (5)$$

$$\eta = \lim_{t \rightarrow \infty} \frac{V}{k_B T} \int_0^t d\tau \left\langle \Pi_{\alpha\beta}(\tau) \cdot \Pi_{\alpha\beta}(0) \right\rangle, \quad (6)$$

where $\Pi_{\alpha\beta}(t)$ refers to the off-diagonal pressure tensor components ($\alpha, \beta = x, y, z$, see references^{71,72} for more details), N is the total number of ions in the simulation box of volume V , N_s the number of ions of species s , k_B the Boltzmann constant and e the elementary charge, m_i is the mass of ion i , $\mathbf{r}_i(t)$ its position, $v_{i\alpha}(t)$ the component α of its velocity, $F_{ij\beta}(t)$ is the component β of the force exerted by ion j on ion i , separated by a distance $r_{ij}(t)$ at time t . The conduction charge z_i is taken as the formal charge, which is usual for simple ionic liquids.⁷³ Note from the equations above that the self-diffusion coefficient D_s , resulting from an average over the N_s ions of a specific species s (sum $\sum_{i=1}^{N_s}$ in Eq. (4)), are calculated with a great accuracy (calculation uncertainty of 1% in this study). On the other hand, the electrical conductivity and the viscosity, as collective observables, are trickier to estimate due to the slow convergence of the corresponding time correlation functions. In the following the values we present for these quantities have an error bar within 5 – 10%.

The temperature and pressure dependence of the transport coefficients can be modeled by an Arrhenius activation law

$$D_s(P, T) = D_s^0 e^{-(E_a^{D_s} + P V_a^{D_s})/RT}, \quad (7)$$

$$\sigma(P, T) = \sigma^0 e^{-(E_a^\sigma + P V_a^\sigma)/RT}, \quad (8)$$

$$\eta(P, T) = \eta^0 e^{-(E_a^\eta + P V_a^\eta)/RT}, \quad (9)$$

where E_a^X is the activation energy associated to the physical quantity X and V_a^X is an activation volume accounting for its pressure dependence.^{1,29,31} The values of X^0 , E_a^X and V_a^X were determined by fitting the molecular dynamics data for the three melts MgCO_3 , CaCO_3 and $\text{CaMg}(\text{CO}_3)_2$ (see Figs. 5, 6, 7, 10, 11). They are given in Table IV for D_s and in Table V for σ and η , for the pressure and temperature range mentioned in Table III.

A. Diffusion coefficient

The diffusivity of calco-magnesian carbonate melts has never been measured and it is only recently that estimations have been provided by the AIMD simulations of Vuilleumier *et al.*²⁹. According to their calculations the diffusion coefficients of Ca and CO_3^{2-} in CaCO_3 along its melting curve (up to 12 GPa) are of comparable magnitude with the ones in purely alkali melts.¹ The agreement between the data of the present MD study and the AIMD

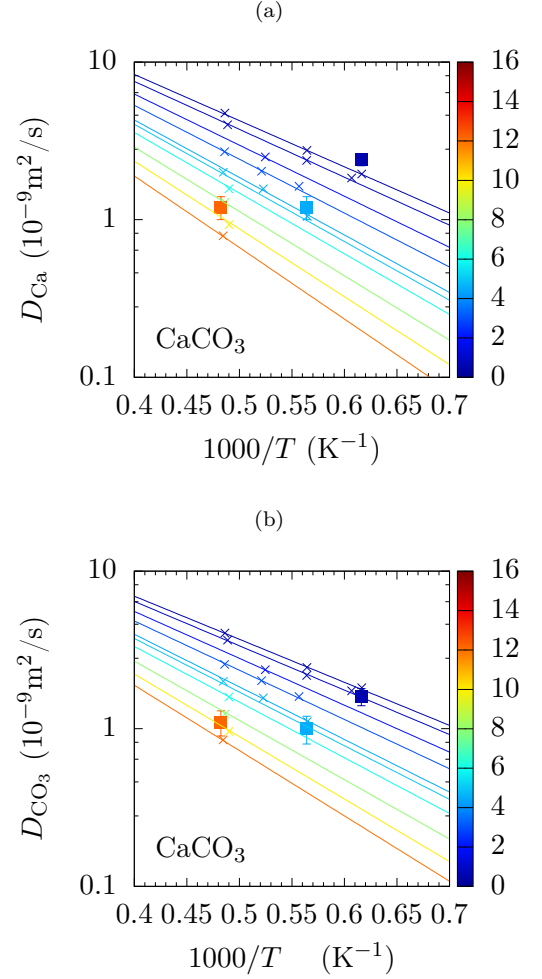


FIG. 5: Diffusion coefficients in CaCO_3 calculated by MD (crosses) and isobaric activation laws obtained by fitting all the simulation points. The AIMD calculations of Vuilleumier *et al.*²⁹ are represented by plain squares. The pressures of the isobars are {0.5, 1, 2, 3, 4.5, 5, 6, 8, 10, 12} in GPa and are referred to with a color code (vertical scale).

simulations of Vuilleumier *et al.*²⁹ is very good at 0.5 and 4.5 GPa, a bit less at 12 GPa where the values of MD are below those of AIMD (Fig. 5). We have also evaluated the diffusion coefficients from our AIMD simulations of MgCO_3 at 4.5 GPa and $\text{CaMg}(\text{CO}_3)_2$ at 2 GPa. In the two cases they are greater than the values issued from MD (Figs. 6 and 7). This is consistent with the slight discrepancy between the two models for the equation of state. Indeed at a given T, P point, the densities yielded by MD simulations are systematically greater than the ones yielded by AIMD (Fig. 3). This means that the free volume of diffusion is smaller in the MD model. By performing a MD simulation of MgCO_3 at the same density as AIMD (1873 K and 2.49 g/cm³), and recalculating the coefficients from this run, we get larger values (namely

	MgCO ₃	CaCO ₃	CaMg(CO ₃) ₂ (left: X=Mg, right: X=Ca)	
$D_{0,X}$ (10^{-9} m ² /s)	117	122	164	150
$E_a^{D,X}$ (kJ/mol)	54	54	58	57
$V_a^{D,X}$ (cm ³ /mol)	$2.5 - 0.07P + 0.0016P^2$	$4.6 - 0.28P + 0.01006P^2$	$3.5 - 0.13P + 0.0029P^2$	$4.6 - 0.28P + 0.0100P^2$
D_{0,CO_3} (10^{-9} m ² /s)	83	86	100	
E_a^{D,CO_3} (kJ/mol)	54	51	54	
V_a^{D,CO_3} (cm ³ /mol)	$2.6 - 0.11P + 0.0036P^2$	$3.3 - 0.08P + 0.0007P^2$	$2.1 - 0.08P + 0.0085P^2$	

TABLE IV: Parameters of the Arrhenius activation law (7) obtained by the interpolation of all MD simulation points. P is in GPa.

$D_{Mg} = 3.11$ and $D_{CO_3} = 2.13 \cdot 10^{-9}$ m²/s, instead of 1.85 and 1.30), but still below the values from AIMD: 4.4 ± 0.5 and $3.5 \pm 0.5 \cdot 10^{-9}$ m²/s, respectively. This could indicate that our empirical force field fails to some extent to describe cohesive forces in every detail. However there is no evidence that AIMD sketches them much more accurately.

The activation energy (51 – 58 kJ/mol) depends little on the ion species (Ca, Mg or CO₃). But it is perceptibly higher than that for alkali melts at 1 bar in which the coulombic forces are weaker.¹ The magnitude of the diffusion coefficients are also slightly smaller in Ca-Mg carbonate melts than in their alkali counterparts. Interestingly if we consider the K₂CO₃-CaCO₃ mixture (at 1 bar and 1100 – 1200 K) D_{Ca} is lower than D_K (by a factor ~ 2) and very close to D_{CO_3} . Moreover, compared to pure K₂CO₃, the presence of the divalent cation decreases D_{CO_3} and D_K by a factor 2 and increases their activation energies by $\sim +50\%$.

B. Electrical Conductivity

As molten salts, carbonate melts are characterized by a high electrical conductivity in the range of $10^1 - 10^3$ S/m, depending on composition, temperature and pressure, which is up to two orders of magnitude more conductive than silicate melts at the same thermodynamic conditions.^{9,25,74} The knowledge of the electrical conductivity of alkali carbonates is crucial for their industrial applications as electrolytes in fuel cell devices. Many experimental and numerical studies have been devoted to this issue. Hence, the electrical conductivity of the end-members and of binary and ternary mixtures of the system Li₂CO₃-Na₂CO₃-K₂CO₃ have been abundantly documented.^{1,65,75,76} Because the addition of small amounts of alkaline-earth carbonates improves the performance of fuel cell devices, in particular in terms of durability,⁷⁷ the electrical conductivity of the Li-K (62–38 mol%) molten carbonate was measured by impedance spectroscopy and found to decrease linearly with small amounts of CaCO₃.³ The electrical conductivity of carbonate melts is not only important for industrial applications, it is also of fundamental interest to understand the conductivity anomalies in the asthenosphere of the Earth's mantle. To address this question, Gail-

lard *et al.*⁹ measured the electrical conductivity of binary and ternary mixtures in the Na-K-Ca system at atmospheric pressure. With regard to Ca-bearing mixtures, MD is in quantitative agreement with their values (deviation of 30% at most), but with a slightly higher activation energy (Fig. 8). Following the work of Gaillard *et al.*⁹, Sifré *et al.*²⁵ studied (up to 3 GPa) Ca and Mg-bearing carbonate compositions: CaCO₃, a natural dolomite (\sim CaMg(CO₃)₂), K₂Mg(CO₃)₂, K₂Ca(CO₃)₂ and Na₂Mg(CO₃)₂. These studies^{9,25} show that the electrical conductivity depends slightly on the chemical composition (see Figs. 8 and 9). The smaller the cation and the lower its charge, the higher is the electrical conductivity.^{25,76} As a consequence, the addition of CaCO₃ or MgCO₃ in a pure alkali carbonate reduces somewhat the conductivity.

Fig. 9 reports the calculated and measured conductivities for CaCO₃ and for the above mentioned Ca or Mg-bearing mixtures at 3 GPa. The agreement is very good for dolomite and for the Na₂Mg(CO₃)₂ mixture. Note that for dolomite at 3 GPa and 1800 K, Yoshino *et al.*⁷⁸ reported an electrical conductivity of 105 S/m, which is almost twice lower than the values of this study and from Sifré *et al.*⁷⁴ Concerning CaCO₃, the calculated and the measured electrical conductivities overlap within uncertainty (e.g. at 3 GPa and 1923 K MD yields 210 ± 10 S/m and Sifré *et al.*²⁵ 230 ± 25 S/m). The agreement between MD and experiments is also good for K₂Ca(CO₃)₂, although it slightly degrades towards low temperatures. Most striking is our disagreement on the K₂Mg(CO₃)₂ mixtures (by a factor $\sim 2 - 3$, Fig. 9), although our force field satisfactorily reproduced the behavior of other Mg-containing mixtures. An explanation could be that this composition is the most dissymmetric one of our study (a small divalent cation coexists with a large monovalent cation in equal proportions). On the other hand, an experimental bias cannot be excluded because this mixture is known for being glass-forming and for easily decomposing.²³

As already emphasized in previous studies, the increase of conductivity with temperature is well fitted by an Arrhenius law with activation energies ranging from 34 to 42 kJ/mol at $P = 1$ atm (Table V). Note that Gaillard *et al.*⁹ found E_a^σ in the range 30 to 35 kJ/mol in alkali-bearing melts and Desmaele *et al.*¹ ~ 20 kJ/mol for purely alkali melts by MD. The conductivity decreases weakly with pressure, which can be accounted for by an

	MgCO ₃	CaCO ₃	CaMg(CO ₃) ₂
σ_0 (S/m)	3842.5	2593.7	4838.7
E_a^σ (kJ/mol)	38	34	42
V_a^σ (cm ³ /mol)	$1.0+0.076P-0.0036P^2$	$2.3+0.048P-0.0041P^2$	$2.7+0.090P-0.0043P^2$
η_0 (Pa·s)	3.9×10^{-4}	2.8×10^{-4}	1.3×10^{-4}
E_a^η (kJ/mol)	37	39	50
V_a^η (cm ³ /mol)	$2.1-0.02P$	$3.6-0.09P$	$3.4-0.05P$

TABLE V: Parameters of the Arrhenius activation laws (8) and (9) for the electrical conductivity and the viscosity, obtained by the interpolation of all MD simulation points. P is in GPa.

increase of the activation energy with P . Hence, we calculated that this energy is between 42 and 51 kJ/mol at 3 GPa depending on the melt composition, whereas Sifré *et al.*²⁵ reported values from 37 to 48 kJ/mol. For dolomite, these authors found an activation energy of 48 kJ/mol, while our calculated value is 41 kJ/mol. That is a fairly good agreement considering that the experimental error on each measurement is about 10%. As for Yoshino *et al.*⁷⁸ they reported a value of 38 kJ/mol at 3 GPa. With regard to the calcite melt (CaCO₃), the activation energy calculated by MD (41 kJ/mol at 3 GPa) is much lower than the value reported by Sifré *et al.*²⁵ (76 kJ/mol at the same pressure), but consistent with the ones they reported for other carbonate compositions (in the range 37 – 48 kJ/mol).

The electrical conductivity estimated from AIMD simulations (this study for CaMg(CO₃)₂ and Vuilleumier *et al.*²⁹ for CaCO₃) are reported on Figs. 10. For CaCO₃ the agreement between MD and AIMD is good at 0.5 GPa but diminishes at higher pressures. As evoked in the case of diffusion coefficients, most of these discrepancies may be related to the small difference between the equation of state provided by the two models. At a given $T - P$, the density is smaller in the AIMD simulations, hence the ionic mobility and the electrical conductivity are higher. For dolomite, given the large uncertainty on the AIMD value ($\sim 50\%$), it can only be stated that the results of the two simulations models (MD and AIMD) are compatible.

Another advantage of the MD approach is that phenomenological relations for transport properties can be tested. It can be shown that the electrical conductivity σ and the diffusion coefficients are linked by a generalized Nernst-Einstein relation, which takes into account the cross correlations between ionic motions, $\sigma = H\sigma^{NE}$ where

$$\sigma^{NE} = \frac{e^2}{k_B T V} \sum_s N_s z_s^2 D_s, \quad (10)$$

with N_s , z_s and D_s are the number, the formal charge and the self diffusion coefficient of ions of atomic species s . The Nernst-Einstein relation assumes that ions move independently from each others. The Haven ratio:

$$H = \frac{\sigma}{\sigma^{NE}} = 1 + \sum_s H_s + \sum_s \sum_{s' \neq s} H_{ss'}, \quad (11)$$

accounts for the average cross correlations (through a scalar product) between the displacements of ions of species s

$$H_s = \lim_{t \rightarrow \infty} \frac{1}{6t} \frac{z_s^2}{\sum_s N_s z_s^2 D_s} \times \sum_{i=1}^{N_s} \sum_{j \neq i}^{N_s} \langle \vec{\Delta}_i^{(s)}(t) \cdot \vec{\Delta}_j^{(s)}(t) \rangle, \quad (12)$$

$$\text{where } \vec{\Delta}_i^{(s)}(t) = \vec{r}_i^{(s)}(t) - \vec{r}_i^{(s)}(0)$$

and the average cross correlations between the displacement of an ion i of species s ($\vec{\Delta}_i^{(s)}$) and that of an ion j of another species s' ($\vec{\Delta}_j^{(s')}$)

$$H_{ss'} = \lim_{t \rightarrow \infty} \frac{1}{6t} \frac{z_s z_{s'}}{\sum_s N_s z_s^2 D_s} \times \sum_{i=1}^{N_s} \sum_{j=1}^{N_{s'}} \langle \vec{\Delta}_i^{(s)}(t) \cdot \vec{\Delta}_j^{(s')}(t) \rangle. \quad (13)$$

The Nernst-Einstein equation is recovered for $H = 1$, although it doesn't imply that H_s and $H_{ss'} \simeq 0$, as these two terms can cancel each other (see Desmaele *et al.*¹). For instance in MgCO₃ (for further details see Table VI), H is close to 1 ($H = 0.92$) although its decomposition gives $H_{\text{Mg}} = -0.14$, $H_{\text{CO}_3} = -0.32$ and $H_{\text{Mg-CO}_3} = 0.38$. Furthermore the fact that both H_{Mg} and H_{CO_3} contributions are negative implies that ions of a same species have a high probability of moving towards opposite directions (see Eq. (12)), which decreases the conductivity. Regarding the cation-anion correlation term, $H_{\text{Mg-CO}_3} = 0.38$, it is positive and almost exactly cancels out the $H_{\text{Mg}} + H_{\text{CO}_3}$ sum. Because Mg and CO₃ ions have charges of opposite signs (see Eq. (13)), $H_{\text{Mg-CO}_3} > 0$ is indicative of an anti-correlation of the displacements of the cations and of the anions, that is to say, they are, on average, moving towards opposite directions, which increases the conductivity. For CaCO₃, an anti-correlation of all the ionic displacements is also observed: a positive contribution of the anion-cation correlation $H_{\text{Ca-CO}_3}$ is not fully overbalanced by the correlations between ions of a same species leading to a Haven ratio less than 1 ($H = 1 + H_{\text{Ca}} + H_{\text{CO}_3} + H_{\text{Ca-CO}_3} = 0.81$). We carried on this approach with some binary mixtures

	T (K)	P (GPa)	σ (S/m)	H	H_{X_1}	H_{X_2}	H_{CO_3}	$H_{X_1-X_2}$	H_{X-CO_3}
MgCO ₃	1823	3.0	245	0.92	-0.14	—	-0.32	—	0.38
CaCO ₃	1773	1.0	220	0.81	-0.22	—	-0.35	—	0.38
MC	1573	3.0	112	0.85	-0.08	0	-0.36	-0.03	0.34
NM	1573	3.0	186	0.87	-0.04	-0.04	-0.29	-0.16	0.40
KM	1573	3.0	75	0.72	-0.10	-0.03	-0.23	-0.22	0.29
KC	1573	3.0	95	0.75	-0.10	-0.05	-0.25	-0.20	0.35

TABLE VI: Haven ratio and its ionic contributions, where X denotes all cations. Note that the error bar on these quantities is of the order of the error bar on the electrical conductivity: $\sim 5 - 10\%$. For mixtures, the notation X_1 ($= \text{Mg, Na or K}$) and X_2 ($= \text{Ca or Mg}$) is the same as the one appearing in the composition name (first column, with M = Mg, C = Ca, N = Na and K = K).

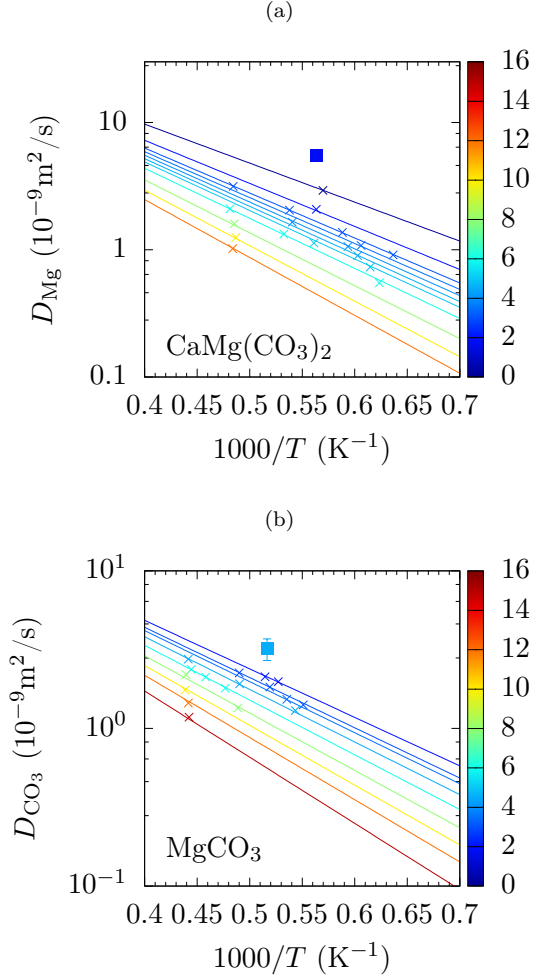


FIG. 6: Diffusion coefficients in MgCO₃ calculated by MD (crosses) and isobaric activation laws obtained by fitting all the simulation points. The AIMD calculations (this study) are represented by plain squares. The pressures of the isobars are $\{2, 3, 3.5, 4.5, 6, 8, 10, 12, 15\}$ in GPa and are referred to with a color code (vertical scale).

(see Table VI), including dolomite. It is worth noticing that the displacements of cations of the same species are mostly not correlated to one another (H_{X_1} and H_{X_2} both ~ 0 , where $X_1, X_2 = \text{Mg, Ca, Na or K}$). However the cross correlations between cationic displacements (as expressed by the term $H_{X_1-X_2}$) seem to depend on the charge of the cations. Indeed, in dolomite $H_{X_1-X_2}$ is close to 0 ($H_{\text{Mg-Ca}} = -0.03$), while in the investigated alkali-alkaline earth mixtures it ranges between -0.16 and -0.22. As for the other terms (H_{CO_3} and H_{X-CO_3}), they give opposite contributions to H (see Table VI). So, although the Nernst-Einstein equation yields, for the melts studied here, a reasonable estimation of the electrical conductivity ($+10 - 30\%$ from the exactly calculated one, σ), it provides no information on the relevance of its underlying assumption (the ions move independently from each other). In fact, as we show it here, its usefulness relies on a cancellation effect between the different ion-ion correlations. As the dependence of this cancellation effect with composition, T or P is non-trivial, we recommend a circumspect use of the Nernst-Einstein approximation.

C. Viscosity

Very little is known on the pressure dependence of the viscosity of molten carbonates. Based on molten salt data reviewed by Janz,⁶⁵ Wolff⁸⁰ roughly estimated an order of magnitude (~ 100 mPa.s) for the viscosity of calcium-rich carbonatites at 973 K and ambient pressure. The ex-situ measurements at mantle pressures ($P = 3$ GPa) made by Sykes *et al.*⁸¹ seem to greatly overestimate the viscosity of dolomitic melts (e.g. for 70:30 mol% CaCO₃-MgCO₃, $\eta = 600$ mPa.s at 1473 K and 1 GPa) in light of the very high activation energy they obtained,²⁴ probably because of an incomplete melting of the sample.⁷⁹ On the other hand, Dobson *et al.*²³ performed the first in-situ measurements of the viscosity of K₂Ca(CO₃)₂ and K₂Mg(CO₃)₂ melts, up to 5.5 GPa, by using the falling sphere method with X-ray radiography. In this pioneering experiment, the temperature was difficult to control and the relative error on viscosity was typically 50%, due to incomplete melting of the

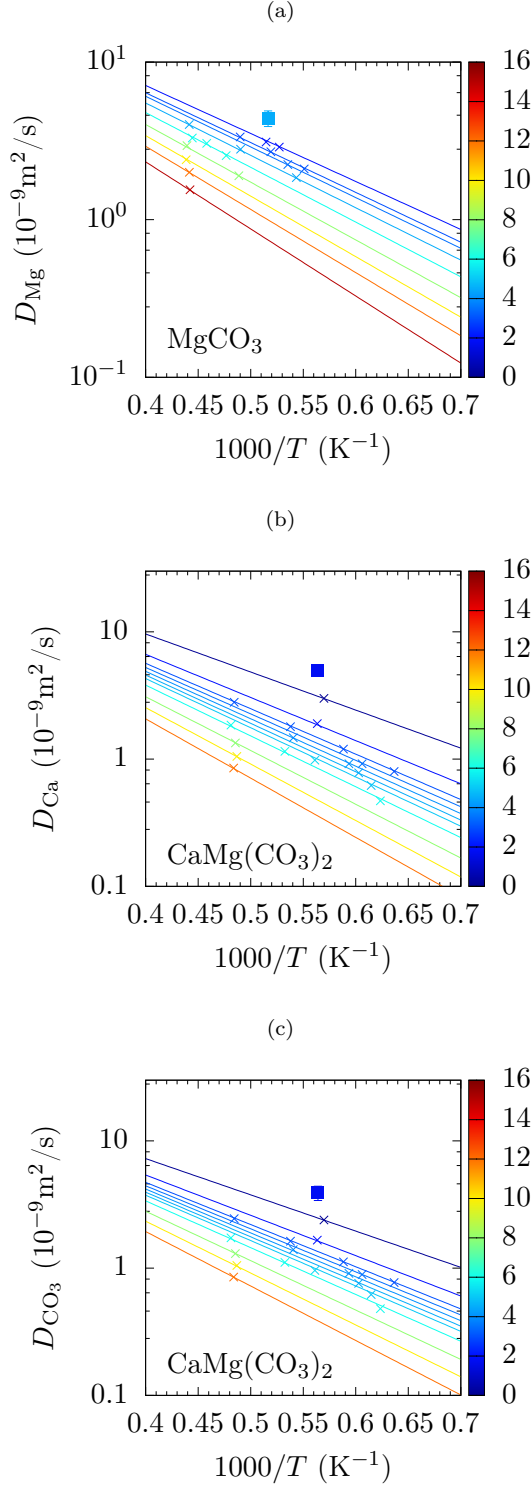


FIG. 7: Diffusion coefficients in $\text{CaMg}(\text{CO}_3)_2$ calculated by MD (crosses) and isobaric activation laws obtained by fitting all the simulation points. The AIMD calculations (this study) are represented by plain squares. The pressures of the isobars are $\{0.1, 2, 3, 3.5, 4, 4.5, 5, 6, 8, 10, 12\}$ in GPa and are referred to with a color code (vertical scale).

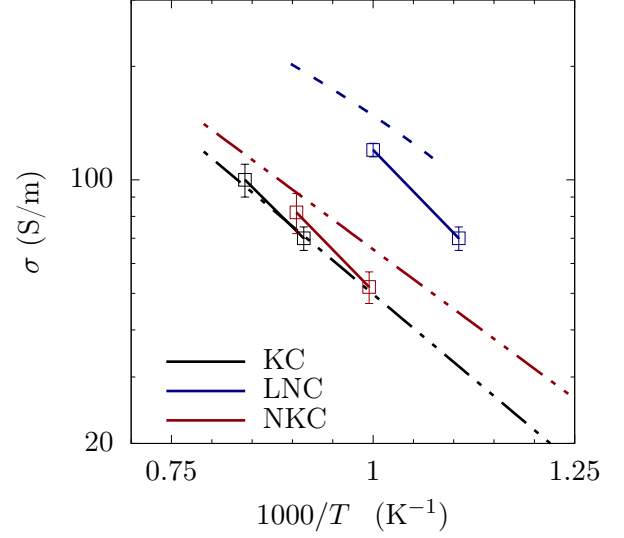


FIG. 8: Electrical conductivity at 1 bar from MD (square and plain lines as a guide to the eye) and from the experiments of Kojima²² (dashed line) and of Gaillard *et al.*⁹ (long dashed and double dotted lines) for $\text{K}_2\text{Ca}(\text{CO}_3)_2$ (KC), $\text{Li}_2\text{Na}_2\text{Ca}(\text{CO}_3)_3$ (LNC) and $\text{Na}_2\text{K}_2\text{Ca}(\text{CO}_3)_3$ (NKC).

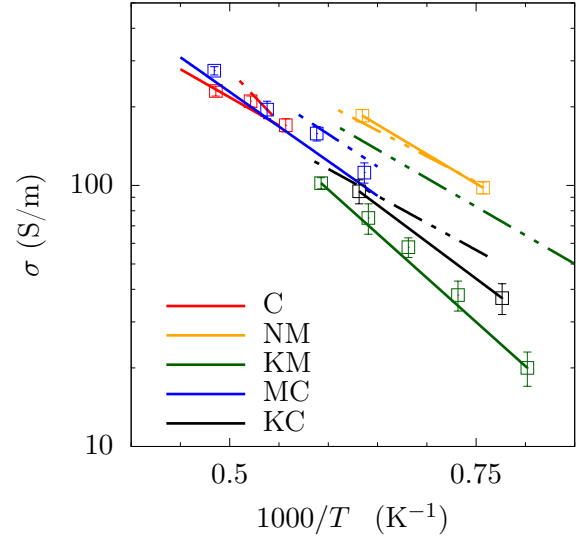


FIG. 9: Electrical conductivity at 3 GPa calculated in MD (square) and measured by Sifré *et al.*²⁵ (dashed line) for CaCO_3 (C) and several equimolar mixtures: $\text{Na}_2\text{Mg}(\text{CO}_3)_2$ (NM), $\text{K}_2\text{Mg}(\text{CO}_3)_2$ (KM), $\text{CaMg}(\text{CO}_3)_2$ (MC) and $\text{K}_2\text{Ca}(\text{CO}_3)_2$ (KC). Plain lines are the Arrhenius activation slopes for C and CM (see Table V) and guides to the eye for NM, KM, NK and KC.

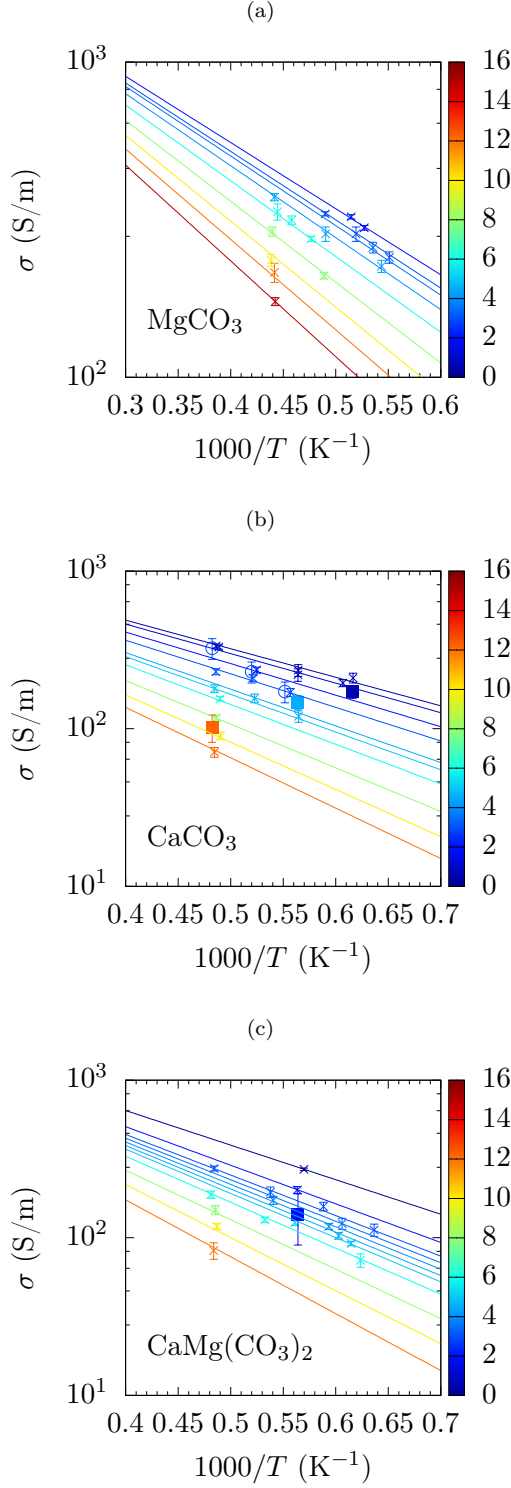


FIG. 10: Electrical conductivity from MD (crosses) and isobaric activation laws (plain lines). The pressures (in GPa) of the isobars are {2, 3, 3.5, 4.5, 6, 8, 10, 12, 15 GPa} for MgCO₃ (top left), {0.5, 1, 2, 3, 4.5, 5, 6, 8, 10, 12 GPa} for CaCO₃ (top right) and {0.1, 2, 3, 3.5, 4, 4.5, 5, 6, 8, 10, 12} for CaMg(CO₃)₂ (bottom) and are referred to with a color code (vertical scale). Estimates from AIMD calculations (this study for CaMg(CO₃)₂ and Vuilleumier *et al.*²⁹ for CaCO₃) are represented by plain squares.

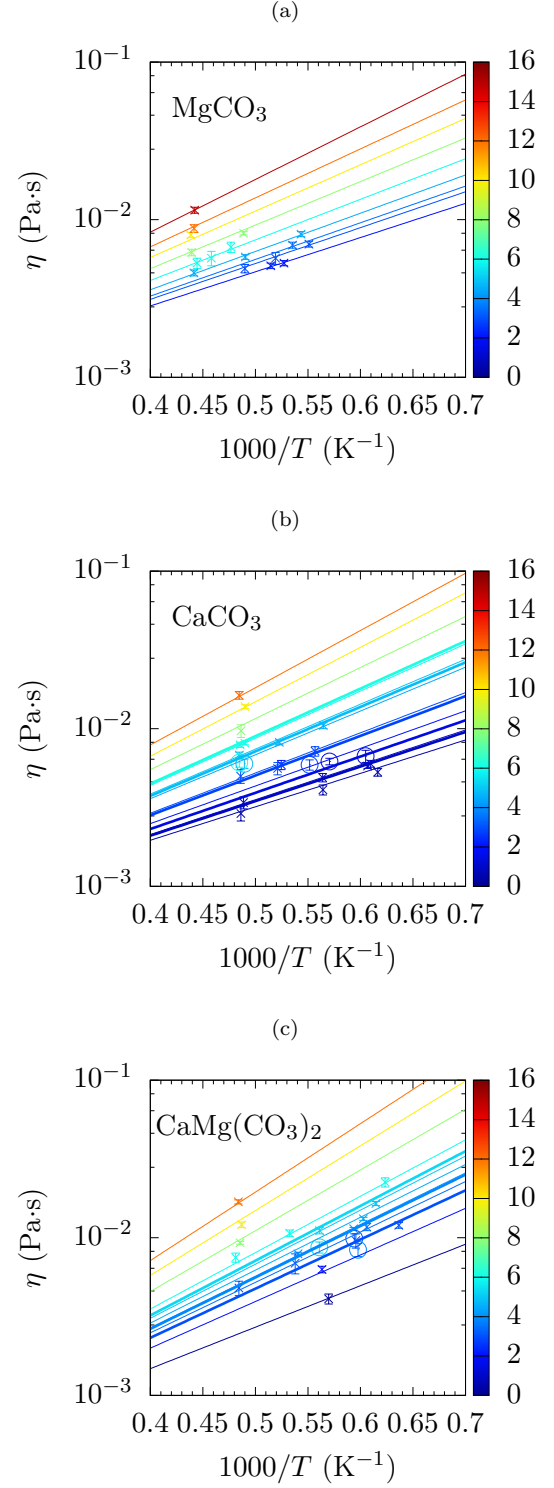


FIG. 11: Viscosity from MD (crosses) and isobaric activation laws (plain lines). The pressures (in GPa) of the isobars are {2, 3, 3.5, 4.5, 6, 8, 10, 12, 15 GPa} for MgCO₃ (top left), {0.5, 1, 2, 3, 4.5, 5, 6, 8, 10, 12 GPa} for CaCO₃ (top right) and {0.1, 2, 3, 3.5, 4, 4.5, 5, 6, 8, 10, 12} for CaMg(CO₃)₂ (bottom) and are referred to with a color code (vertical scale). The data recently reported by Kono *et al.*²⁴ are plotted as circles, the corresponding isobars (0.9, 1.5, 2.8, 4.8 and 6.2 GPa for CaCO₃ and 3.0, 3.9 and 5.3 GPa for CaMg(CO₃)₂) obtained from the present MD study are reported for comparison (bold blue lines).

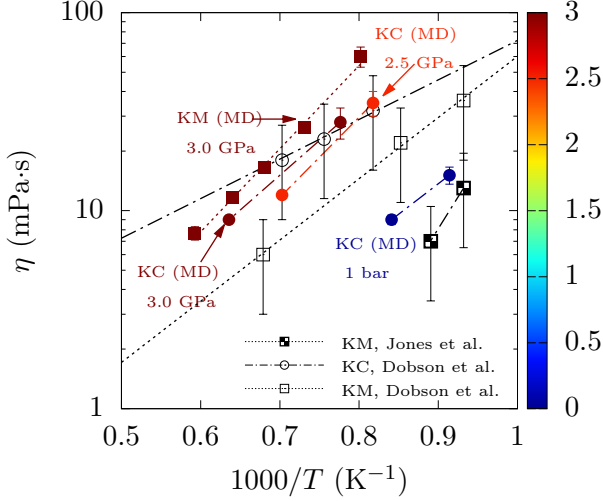


FIG. 12: Viscosity calculated by MD (plain symbols) and measured by Dobson *et al.*²³ (empty symbols) and by Jones *et al.*⁷⁹ (half-empty symbols) for $\text{K}_2\text{Ca}(\text{CO}_3)_2$ (KC, circles) and $\text{K}_2\text{Mg}(\text{CO}_3)_2$ (KM, squares). The color code refers to the pressure as indicated by the vertical scale (in GPa).

sample and to convection effects at the highest temperatures. Besides the limited frame rate used to capture the images of the falling sphere greatly reduces the accuracy of the final velocity measurement, which is crucial for determining the viscosity.²⁴ Nevertheless it was found that Ca, Mg-bearing carbonates under high $T-P$ have a viscosity similar to that of alkali carbonates at 1 bar (6 – 36 mPa·s in the range 2.5 – 5.5 GPa). This qualitative observation is consistent with the results of our MD calculations (see Fig. 11). However we do not agree with the assertion of the authors²³ that the effect of pressure on viscosity is negligible in the pressure range investigated (up to 5.5 GPa) and we think that this observation results from the large error bars of the study ($\sim 50\%$ on η and ± 0.5 GPa on P , see also the discrepancy with the first results of Jones *et al.*⁷⁹). We calculated the viscosity of $\text{K}_2\text{Ca}(\text{CO}_3)_2$ at 0, 2.5 and 3 GPa and the viscosity of $\text{K}_2\text{Mg}(\text{CO}_3)_2$ at 3 GPa. The viscosity depends strongly on the temperature by following an Arrhenius law with an activation energy a little higher for $\text{K}_2\text{Mg}(\text{CO}_3)_2$ than for $\text{K}_2\text{Ca}(\text{CO}_3)_2$. Even at these moderate pressures it is obvious that the activation energy depends on pressure (Fig. 12), in contrast with the observation of Dobson *et al.*²³. At a given pressure, we obtained similar activation energies for the two compositions $\text{K}_2\text{Mg}(\text{CO}_3)_2$ and $\text{K}_2\text{Ca}(\text{CO}_3)_2$ (~ 80 kJ/mol at 3 GPa). However these activation energies differ from the ones calculated for the end-members CaCO_3 and MgCO_3 (43 – 49 kJ/mol), for dolomite (60 kJ/mol) and for alkali melts (31 – 39 kJ/mol)¹ at the same pressure. This

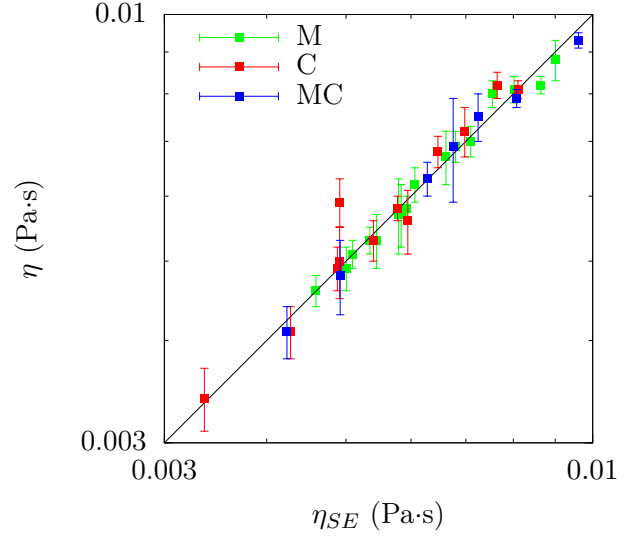


FIG. 13: Comparison of the viscosity calculated using the Green-Kubo formula, η , and the Stokes-Einstein equation, η_{SE} , at all T and P . The d parameter, figuring in Eq. (14) has been adjusted for MgCO_3 (M), CaCO_3 (C) and $\text{CaMg}(\text{CO}_3)_2$ (MC) to 3.2, 3.5 and 3.4 Å, respectively, so as to align the data on the $\eta = \eta_{SE}$ bisector (black line).

illustrates that the viscosity not only depends on the temperature, but also on the chemical composition. Recently, Kono *et al.*²⁴ have reported viscosities of calcite and dolomitic ($\text{Mg}_{0.40}\text{Fe}_{0.09}\text{Ca}_{0.51}\text{CO}_3$) melts at temperatures just above the melting point up to 6.2 GPa, by using the falling sphere method with a powerful technique of ultra-fast synchrotron X-ray imaging. The measured viscosities (6 – 10 mPa·s, with an error of 9%) are of the same order of magnitude as those of Dobson *et al.*²³, although the composition and the temperature differ in the two studies. The values of Kono *et al.*²⁴ (at 0.9 – 6.2 GPa and 1653 – 2063 K for calcite, 3.0 – 5.3 GPa and 1683 – 1783 K for dolomite) are reported on Fig. 11. For calcite a satisfying agreement (within 10 – 15%, i.e. within the overlap of error bars) is found with our calculations, better than with the values of Vuilleumier *et al.*²⁹ For dolomite the agreement, although comprised between 3 and 30%, is reasonable once considered some anomalous trend in the experimental data. Indeed the viscosities measured by Kono *et al.*²⁴ at 3.9 GPa and $1000/T \sim 0.6$ is lower than the one measured at 3.0 GPa at the same temperature, whereas the viscosity is expected to increase upon increasing pressure. Incidentally, we do not think that the small content (9 mol%) of FeCO_3 in the experimental composition has a significant contribution to the viscosity and could account for the MD-experiment discrepancy.

For natrocarbonatite (Natro, $\text{Na}_{1.1}\text{K}_{0.18}\text{Ca}_{0.36}\text{CO}_3$) at 1 bar and 823 K (near eruption conditions at the Ol

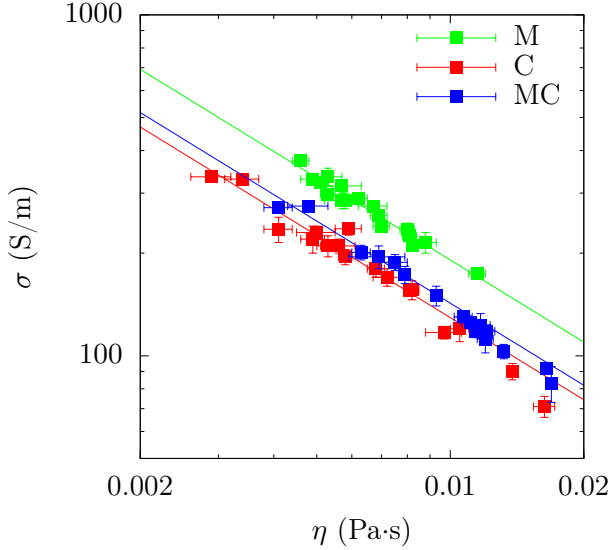


FIG. 14: Electrical conductivity as a function of viscosity. The squares are the MD data and the lines are empirical fits of the MD data by equation $\sigma = A/\eta^{0.8}$ (where σ is in S/m and η in Pa·s) with $A = 4.78, 3.25$ and 3.58 for CaCO_3 (C), MgCO_3 (M) and $\text{CaMg}(\text{CO}_3)_2$ (MC), respectively.

Doinyo Lengai volcano), we calculated a viscosity of 68 ± 10 mPa·s. We believe this is a more reliable value than the estimation given by Treiman and Schedl⁸² using molten salt data (5 mPa·s), which seems rather low for a Ca-bearing mixture at relatively low temperature. For example compared with the alkali ternary eutectic mixture ($\text{Li}_{0.435}\text{Na}_{0.315}\text{K}_{0.25}\text{CO}_3$) the viscosity of natro-carbonatite is greater by a factor ~ 3 according to our MD calculations.¹ This is consistent with the observations made by both experiments and simulations, of a decrease of the ionic conductivity upon addition of the alkaline-earth cation Ca.^{3,9} Interestingly the calculated viscosity is much lower than the ones measured by Norton and Pinkerton⁸³ for several carbonatitic melts issued from the eruption of Ol Doinyo Lengai in 1988. At 823 K, the measured viscosities vary a lot ($10^2 - 10^4$ mPa/s) as a result of varying compositions (with or without a silicate component), crystallinity (presence of crystals of various sizes) and vesicularity (presence of CO_2 bubbles). Consequently, for a composition close to the one we studied ($\text{Na}_{1.1}\text{K}_{0.18}\text{Ca}_{0.36}\text{CO}_3$), they reported a viscosity as high as ~ 600 mPa·s. At variance with experiments where a complete melting is uneasy to assess, the MD value (68 ± 10 mPa·s) is representative of carbonate melts. Besides, this oil-like viscosity is consistent with field observations where effusion of a very fluid lava is seen (see the videos of Fischer *et al.*⁸⁴ with the link of reference 85).

To obtain a phenomenological description of the viscosity of simple liquids, the Stokes-Einstein equation is often

used

$$\eta_{SE} = \frac{k_B T}{2\pi D d}, \quad (14)$$

where d is the diameter of the diffusing particle and D its diffusion coefficient. In the present case, the latter is assumed to be given by the arithmetic mean of the diffusion coefficients, $D = \sum_s x_s D_s / \sum_s x_s$ where x_s is the molar fraction of ion of species s in the melt. We chose $d = 3.2, 3.5$ and 3.4 Å for MgCO_3 , CaCO_3 and $\text{CaMg}(\text{CO}_3)_2$ respectively. The behavior of the MD-calculated viscosity with pressure and temperature was very well reproduced by Eq. (14) using these parameters (Fig. 13). To calculate the hydrodynamic diameter in a more grounded framework we used the following expression: $d = x_X^2 d_{XX} + x_{\text{CO}_3}^2 d_{\text{CO}_3\text{CO}_3} + 2x_X x_{\text{CO}_3} d_{X\text{CO}_3}$, where x_X and x_{CO_3} are the molar fractions of cation X and of anion CO_3 , respectively, and d_{XX} , $d_{\text{CO}_3\text{CO}_3}$ and $d_{X\text{CO}_3}$ the cation-cation, carbonate-carbonate and cation-carbonate distances issued from the closest approach distances indicated by the corresponding PDFs (in fact, the d parameters correspond to the distances at which the integral of the PDFs is equal to 1). This ansatz leads to $d = 3.1, 3.4$ and 3.3 Å for MgCO_3 , CaCO_3 and $\text{CaMg}(\text{CO}_3)_2$ respectively. These values are almost identical (-0.1 Å) to the ones obtained by fitting the values of d to Eq. (14).

Finally, the electrical conductivity σ (in S/m) and the viscosity η (in Pa·s) can be related by the following empirical formula:

$$\sigma = \frac{A}{\eta^{0.8}}, \quad (15)$$

where $A = 4.80, 3.25$ and 3.58 for MgCO_3 , CaCO_3 and $\text{CaMg}(\text{CO}_3)_2$ respectively (Fig. 14). A comparable relation between these two transport coefficients has been also highlighted experimentally and computationally for various melt compositions.^{1,25,29}

V. CONCLUSION

Following our previous work on the Li_2CO_3 – Na_2CO_3 – K_2CO_3 melts, we have studied the thermodynamics, the microscopic structure and the transport properties (diffusion coefficients, electrical conductivity and viscosity) of Ca and Mg-bearing carbonate melts up to 2073 K and 15 GPa. For that we have developed an empirical force field benchmarked on data from experiments (density of the rhombohedral crystal phases at 300 K and up to 4 GPa, and the density and the compressibility of the $\text{K}_2\text{Ca}(\text{CO}_3)_2$ melt) and from AIMD simulations (microscopic structure of five liquids). The density and compressibility, evaluated for the metastable melts of MgCO_3 and CaCO_3 at 1100 K and 1 bar, are in very good agreement with the estimates of the experimental literature. Moreover we have shown that alkaline-earth carbonate

mixtures behave ideally regarding the density and the compressibility. Based on the example of a Na–Ca–K melt (natrocarbonatite), the assumption of an ideal behavior for alkali-alkaline-earth mixtures seems a little less accurate but still reasonable.

The equations of state of carbonate melts with a composition of prior interest in the study of the Earth’s mantle (MgCO_3 , CaCO_3 and $\text{CaMg}(\text{CO}_3)_2$), as well as that modeling the natrocarbonatite emitted at the Ol Doinyo Lengai volcano ($\text{Na}_{1.10}\text{K}_{0.18}\text{Ca}_{0.36}\text{CO}_3$), were evaluated and modeled by a third-order Birch-Murnaghan formula. Covering a large T , P range, these data may help in the debate on the geodynamics of carbonatitic melts relative to silicate melts.⁸⁶

The analysis of the PDFs associated to the dolomitic melt showed an ideal behavior of the microscopic structure, as the PDFs in $\text{CaMg}(\text{CO}_3)_2$ are similar to the corresponding ones in CaCO_3 and in MgCO_3 . Moreover, no major modification of the structure was observed with increasing pressure.

As for the transport properties (diffusion coefficients, electrical conductivity and viscosity), they evolve smoothly (Arrhenius-like) over the studied $T - P$ domain. Thus at the high $T - P$ conditions of the Earth’s mantle, Mg and Ca-bearing molten carbonates keep the main features of molten salts, namely the ions are highly mobile. For example the viscosity is comprised in the range 1 – 100 mPa·s, that is in between the one of water and the one of olive oil at room conditions. However, the composition has a non negligible effect on transport coefficients: calco-magnesian melts are systematically more viscous than their alkali counterparts. These results may provide new insights into magmatic processes implying carbonatitic melts.^{80,82,87}

Finally we discussed the reliability of the phenomenological Nernst-Einstein and the Stokes-Einstein equations, that relate the diffusion coefficients to the electrical conductivity and to the viscosity, respectively. These relations are often used to infer one of the transport coefficient from another one that has been measured. According to the present study, both formulas lead to reasonable values. However the underlying assumptions of the relations are not always representative of the transport mechanism itself. We have shown that the fairly good predictions provided by the Nernst-Einstein equation (which assumes that the ions move independently from one another) result from a partial cancellation of interionic dynamic correlations whose dependence with composition, T or P is non-trivial. As a consequence we recommend a circumspect use of the Nernst-Einstein approximation.

In summary, the overall agreement between the results of the MD simulations using this force field and the full set of available experimental data (thermodynamics and transport coefficients) provides evidence of the ability of our FF to describe with accuracy the properties of any melt in the MgCO_3 – CaCO_3 – Li_2CO_3 – Na_2CO_3 – K_2CO_3 system.

SUPPLEMENTARY MATERIAL

See supplementary material for the density of crystal phases calculated by anisotropic relaxation of the rhombohedral structures up to 4 GPa, the evolution of the PDFs issued by MD with increasing pressure (up to 15 GPa), a summary of all calculated properties with their uncertainties.

ACKNOWLEDGMENTS

The research leading to these results has received funding from the Région Ile-de-France and the European Communitys Seventh Framework Program (FP7/2007-2013) under Grant agreement (ERC, N° 279790). The authors acknowledge GENCI for HPC resources (Grant No. 2015-082309).

- ¹E. Desmaele, N. Sator, R. Vuilleumier, and B. Guillot, *J. Chem. Phys.* **150**, 094504 (2019).
- ²E. Desmaele, *Physicochemical Properties of Molten Carbonates from Atomistic Simulations*, Ph.D. thesis, Sorbonne Université (2017).
- ³V. Lair, V. Albin, A. Ringued, and M. Cassir, *Int. J. Hydrogen Energy* **37**, 19357 (2012).
- ⁴D. Chery, V. Lair, and M. Cassir, *Electrochim. Acta* **160**, 74 (2015).
- ⁵D. Chery, V. Lair, and M. Cassir, *Front. Energy Res.* **3**, 43 (2015).
- ⁶M. Cassir, S. McPhail, and A. Moreno, *Int. J. Hydrogen Energy* **37**, 19345 (2012).
- ⁷M. Cassir, A. Ringued, and V. Lair, in *Molten Salts Chemistry*, edited by F. Lantelme and H. Groult (Elsevier, Oxford, 2013).
- ⁸R. Dasgupta and M. M. Hirschmann, *Nature* **440**, 659 (2006).
- ⁹F. Gaillard, M. Malki, G. Iacono-Marziano, M. Pichavant, and B. Scaillet, *Science* **322**, 1363 (2008).
- ¹⁰R. Dasgupta and M. M. Hirschmann, *Earth Planet. Sci. Lett.* **298**, 1 (2010).
- ¹¹R. Dasgupta, *Rev. Mineral. Geochem.* **75**, 183 (2013).
- ¹²T. Hammouda and S. Keshav, *Chem. Geol.* **418**, 171 (2015).
- ¹³R. H. Mitchell, *Can. Mineral.* **43**, 2049 (2005).
- ¹⁴A. Woolley and B. Kjarsgaard, “Carbonatite Occurrences of the World: Map and Database. Geological Survey of Canada. Open File 5796,” (2008).
- ¹⁵J. Keller and A. N. Zaitsev, *Lithos* **148**, 45 (2012).
- ¹⁶A. R. Woolley and A. A. Church, *Lithos* **85**, 1 (2005).
- ¹⁷A. V. Spivak, Y. A. Litvin, S. V. Ovsyannikov, N. A. Dubrovinskaia, and L. S. Dubrovinsky, *J. Solid State Chem.* **191**, 102 (2012).
- ¹⁸N. A. Solopova, Y. A. Litvin, A. V. Spivak, N. A. Dubrovinskaia, L. S. Dubrovinsky, and V. S. Urusov, *Dokl. Earth Sci.* **453**, 1106 (2013).
- ¹⁹N. A. Solopova, L. Dubrovinsky, A. V. Spivak, Y. A. Litvin, and N. Dubrovinskaia, *Phys. Chem. Miner.* **42**, 73 (2015).
- ²⁰A. J. Irving and P. J. Wyllie, *Geochim. Cosmochim. Acta* **39**, 35 (1975).
- ²¹K. Suito, J. Namba, T. Horikawa, Y. Taniguchi, N. Sakurai, M. Kobayashi, A. Onodera, O. Shimomura, and T. Kikegawa, *Am. Mineral.* **86**, 997 (2001).
- ²²T. Kojima, *Physical and Chemical Properties of Molten Carbonates*, Ph.D. thesis, Kobe University (2009).
- ²³D. P. Dobson, A. P. Jones, R. Rabe, T. Sekine, K. Kurita, T. Taniguchi, T. Kondo, T. Kato, O. Shimomura, and S. Urakawa, *Earth Planet. Sci. Lett.* **143**, 207 (1996).

- ²⁴Y. Kono, C. Kenney-Benson, D. Hummer, H. Ohfuji, C. Park, G. Shen, Y. Wang, A. Kavner, and E. Manning C., *Nat. Commun.* **5**, 5091 (2014).
- ²⁵D. Sifré, L. Hashim, and F. Gaillard, *Chem. Geol.* **418**, 189 (2015).
- ²⁶S. M. Hurt and R. A. Lange, *Geochim. Cosmochim. Acta*, 123 (2019).
- ²⁷Z. Zhang and Z. Liu, *Chin. J. Geochem.* **34**, 13 (2015).
- ²⁸Z. Li, J. Li, R. Lange, J. Liu, and B. Militzer, *Earth Planet. Sci. Lett.* **457**, 395 (2017).
- ²⁹R. Vuilleumier, A. Seitsonen, N. Sator, and B. Guillot, *Geochim. Cosmochim. Acta* **141**, 547 (2014).
- ³⁰X. Du, M. Wu, J. S. Tse, and Y. Pan, *ACS Earth and Space Chem.* **2**, 1 (2018).
- ³¹D. Corradini, C. F.-X., and R. Vuilleumier, *J. Chem. Phys.* **144**, 104507 (2016).
- ³²Q. Liu and R. Lange, *Contrib. Mineral. Petrol.* **146**, 370 (2003).
- ³³J. Hudspeth, C. Sanloup, and Y. Kono, *Geochem. Perspect. Lett.* **7**, 17 (2018).
- ³⁴P. S. Yuen, M. W. Lister, and S. C. Nyburg, *J. Chem. Phys.* **68**, 1936 (1978).
- ³⁵M. T. Dove, B. Winkler, M. Leslie, M. J. Harris, and E. K. H. Salje, *Am. Mineral.* **77**, 244 (1992).
- ³⁶A. Pavese, M. Catti, G. D. Price, and R. A. Jackson, *Phys. Chem. Miner.* **19**, 80 (1992).
- ³⁷A. Pavese, M. Catti, S. C. Parker, and A. Wall, *Phys. Chem. Miner.* **23**, 89 (1996).
- ³⁸D. K. Fislser, J. D. Gale, and R. T. Cygan, *Am. Mineral.* **85**, 217 (2000).
- ³⁹T. D. Archer, S. E. A. Birse, M. T. Dove, S. A. T. Redfern, J. D. Gale, and R. T. Cygan, *Phys. Chem. Miner.* **30**, 416 (2003).
- ⁴⁰P. Raiteri, J. D. Gale, D. Quigley, and P. M. Rodger, *J. Phys. Chem. C* **114**, 5997 (2010).
- ⁴¹M. Born and K. Huang, *Dynamical Theory of Crystal Lattices* (Clarendon press, 1954).
- ⁴²M. J. Genge, G. D. Price, and A. P. Jones, *Earth Planet. Sci. Lett.* **131**, 225 (1995).
- ⁴³S. M. Hurt and A. S. Wolf, *Phys. Chem. Miner.* **46**, 165 (2018).
- ⁴⁴J. VandeVondele, M. Krack, F. Mohamed, M. Parrinello, T. Chassaing, and J. Hutter, *Comput. Phys. Commun.* **167**, 103 (2005).
- ⁴⁵G. Lippert, J. Hutter, and M. Parrinello, *Mol. Phys.* **92**, 477 (1997).
- ⁴⁶J. VandeVondele, F. Mohamed, M. Krack, J. Hutter, M. Sprik, and M. Parrinello, *J. Chem. Phys.* **122**, 101 (2005).
- ⁴⁷J. VandeVondele and J. Hutter, *J. Chem. Phys.* **127**, 114105 (2007).
- ⁴⁸S. Goedecker, M. Teter, and J. Hutter, *Phys. Rev. B* **54**, 1703 (1996).
- ⁴⁹C. Hartwigsen, S. Goedecker, and J. Hutter, *Phys. Rev. B* **58**, 3641 (1998).
- ⁵⁰M. Krack, *Theor. Chem. Acc.* **114**, 145 (2005).
- ⁵¹D. Becke A., *Phys. Rev. A* **38**, 3098 (1988).
- ⁵²C. Lee, W. Yang, and G. Parr R., *Phys. Rev. B* **37**, 785 (1988).
- ⁵³S. Grimme, J. Antony, S. Ehrlich, and H. Krieg, *J. Chem. Phys.* **132**, 154104 (2010).
- ⁵⁴S. Nosé, *Mol. Phys.* **52**, 255 (1984).
- ⁵⁵S. Nosé, *J. Chem. Phys.* **81**, 511 (1984).
- ⁵⁶W. Smith and T. Forester, *J. Mol. Graphics* **14**, 136 (1996).
- ⁵⁷S. A. T. Redfern, B. J. Wood, and C. M. B. Henderson, *Geophys. Res. Lett.* **20**, 2099 (1993).
- ⁵⁸G. Fiquet, F. Guyot, and J.-P. Itie, *Am. Mineral.* **79**, 15 (1994).
- ⁵⁹J. Zhang, I. Martinez, F. Guyot, P. Gillet, and S. K. Saxena, *Phys. Chem. Miner.* **24**, 122 (1997).
- ⁶⁰N. L. Ross, *Am. Mineral.* **82**, 682 (1997).
- ⁶¹M. C. O'Leary, R. A. Lange, and Y. Ai, *Contrib. Mineral. Petrol.* **170**, 3 (2015).
- ⁶²S. M. Antao and I. Hassan, *Can. Mineral.* **48**, 1225 (2010).
- ⁶³A. Buob, R. W. Luth, M. W. Schmidt, and P. Ulmer, *Am. Mineral.* **91**, 435 (2006).
- ⁶⁴A. Shatskiy, K. Litasov, and Y. Palyanov, *Russ. Geol. Geophys.* **56**, 113 (2015).
- ⁶⁵G. J. Janz, *J. Phys. Chem. Ref. Data* **17** (Suppl. 2) (1988).
- ⁶⁶S. A. Markgraf and R. J. Reeder, *Am. Mineral.* **70**, 590 (1985).
- ⁶⁷R. M. Hazen, R. T. Downs, A. P. Jones, and L. Kah, *Rev. Mineral. Geochem.* **75**, 7 (2013).
- ⁶⁸M. C. O'Leary, R. A. Lange, and Y. Ai, in *AGU Fall Meeting Abstracts*, Vol. 1 (2009).
- ⁶⁹F. Birch, *Phys. Rev.* **71**, 809 (1947).
- ⁷⁰S. Kohara, S. Badyal Y., N. Koura, Y. Idemoto, S. Takahashi, L. A. Curtiss, and M.-L. Saboungi, *J. Phys.: Condens. Matter* **10**, 3301 (1998).
- ⁷¹M. P. Allen and D. J. Tildesley, *Computer Simulation of Liquids* (Clarendon Press, New York, NY, USA, 1989).
- ⁷²B. Hess, *J. Chem. Phys.* **116**, 209 (2002).
- ⁷³E. M. Adams, I. R. McDonald, and K. Singer, *Proc. R. Soc. A* **357**, 37 (1977).
- ⁷⁴D. Sifré, E. Gardés, M. Massuyeau, L. Hashim, S. Hier-Majumder, and F. Gaillard, *Nature* **509**, 81 (2014).
- ⁷⁵T. Kojima, Y. Miyazaki, K. Nomura, and K. Tanimoto, *J. Electrochem. Soc.* **154**, F222 (2007).
- ⁷⁶T. Kojima, Y. Miyazaki, K. Nomura, and K. Tanimoto, *J. Electrochem. Soc.* **155**, F150 (2008).
- ⁷⁷T. Kojima, Y. Miyazaki, K. Nomura, and K. Tanimoto, *J. Electrochem. Soc.* **150**, E535 (2003).
- ⁷⁸T. Yoshino, E. McIsaac, M. Laumonier, and T. Katsura, *Phys. Earth Planet. Inter.* **194**, 1 (2012).
- ⁷⁹A. P. Jones, D. Dobson, and M. Genge, *Geol. Mag.* **132**, 121 (1995).
- ⁸⁰J. A. Wolff, *Geol. Mag.* **131**, 145 (1994).
- ⁸¹D. Sykes, M. B. Baker, and P. J. Wyllie, in *Abstracts, AGU Spring Meeting*, Vol. 73 (1992) p. 372.
- ⁸²A. H. Treiman and A. Schedl, *J. Geol.* **91**, 437 (1983).
- ⁸³G. Norton and H. Pinkerton, *Eur. J. Mineral.* **9**, 351 (1997).
- ⁸⁴T. Fischer, P. Burnard, B. Marty, D. Hilton, E. Fri, F. Palhol, Z. Sharp, and F. Mangasini, *Nature* **459**, 77 (2009).
- ⁸⁵NSF, "Alchemy in Tanzania? Gas Becomes Solid at Surface of Oldoinyo Lengai Volcano," (2009), [accessed 03.25.2019].
- ⁸⁶Q. Liu, T. J. Tenner, and R. A. Lange, *Contrib. Mineral. Petrol.* **153**, 55 (2007).
- ⁸⁷A. H. Treiman, "Carbonatites - Genesis and Evolution," (Unwin-Hyman, London, 1989) Chap. Carbonatite Magma: Properties and Processes, p. 89.

**Supplementary Material for "The $\text{MgCO}_3\text{--CaCO}_3\text{--Li}_2\text{CO}_3\text{--Na}_2\text{CO}_3\text{--K}_2\text{CO}_3$
Carbonate Melts: Thermodynamics and Transport Properties by Atomistic
Simulations"**

Elsa Desmaele,^{1, a)} Nicolas Sator,¹ Rodolphe Vuilleumier,² and Bertrand Guillot^{1, b)}

¹⁾*Sorbonne Université, CNRS, Laboratoire de Physique*

*Théorique de la Matière Condensée, LPTMC, F75005, Paris,
France*

²⁾*PASTEUR, Département de chimie, École normale supérieure,
PSL University, Sorbonne Université, CNRS, 75005 Paris,
France*

(Dated: 2 July 2022)

^{a)}Electronic mail: elsa.desmaele@gmail.com

^{b)}Electronic mail: guillot@lptmc.jussieu.fr

CONTENTS

List of Figures	2
List of Tables	2
References	13

LIST OF FIGURES

S1	Pressure evolution of PDFs for MgCO_3	5
S2	Pressure evolution of PDFs for CaCO_3	6
S3	Pressure evolution of PDFs for $\text{CaMg}(\text{CO}_3)_2$	7

LIST OF TABLES

S1	Crystal structure parameters for MgCO_3	3
S2	Crystal structure parameters for CaCO_3 and $\text{CaMg}(\text{CO}_3)_2$	4
S3	Summary of the calculated properties for MgCO_3	8
S4	Summary of the calculated properties for CaCO_3	9
S5	Summary of the calculated properties for $\text{CaMg}(\text{CO}_3)_2$	10
S6	Summary of the calculated properties for binary mixtures	11
S7	Summary of the calculated properties for ternary mixtures	12

		$P(\text{GPa})$	$n \text{ (g/cm}^3\text{)}$	$a \text{ (\AA)}$	$b \text{ (\AA)}$	$c \text{ (\AA)}$	$\gamma \text{ (}^\circ\text{)}$
<hr/>							
MgCO_3							
MD	0	3.04	4.60	4.60	15.07	120.0	
Exp. ^{S1}	0	3.01	4.64	15.02	120		
Exp. ^{S2}	0	3.02	4.64	14.96	120		
Exp. ^{S3}	0	3.00	4.64	15.03	120		
Exp. ^{S4}	0	3.01	4.64	15.01	120		
Exp. ^{S5}	0	3.01	4.63	15.02	120		
MD	2	3.07	4.58	4.58	14.91	120.0	
Exp. ^{S4}	2	3.06	4.62	14.91	120		
Exp. ^{S2}	2	3.03	4.63	14.95	120		
Exp. ^{S3}	2	3.06	4.62	14.91	120		
Exp. ^{S5}	2	3.06	4.62	14.88	120		
MD	4	3.15	4.57	4.57	14.77	119.8	
Exp. ^{S4}	4	3.12	4.59	14.75	120		
Exp. ^{S2}	4	3.06	4.62	14.80	120		
Exp. ^{S3}	4	3.09	4.60	14.82	120		
Exp. ^{S5}	4	3.11	4.60	14.75	120		
<hr/>							

TABLE S1. Crystal structure parameters for rhombohedral MgCO_3 at 300 K from the experimental literature (Exp.) and calculated by anisotropic MD simulations (NST ensemble).

	$P(\text{GPa})$	$n \text{ (g/cm}^3\text{)}$	$a \text{ (\AA)}$	$b \text{ (\AA)}$	$c \text{ (\AA)}$	$\gamma \text{ (}^\circ\text{)}$
<hr/>						
CaCO ₃						
MD	0	2.63	5.04	5.04	17.23	120.0
Exp. ^{S1}	0	2.71	4.99		17.06	120
<hr/>						
CaMg(CO ₃) ₂						
MD	0	2.84	4.84	4.84	16.00	120.0
Exp. ^{S3}	0	2.84	4.83		16.01	120
<hr/>						
MD	2	2.91	4.81	4.81	15.74	120.0
Exp. ^{S3}	2	2.89	4.81		15.87	120
<hr/>						
MD	4	2.97	4.80	4.80	15.51	120.2
Exp. ^{S3}	4	2.94	4.79		15.74	120
<hr/>						

TABLE S2. Crystal structure parameters for rhombohedral CaCO₃ and CaMg(CO₃)₂ at 300 K from the experimental literature (Exp.) and calculated by anisotropic MD simulations (*NST* ensemble).

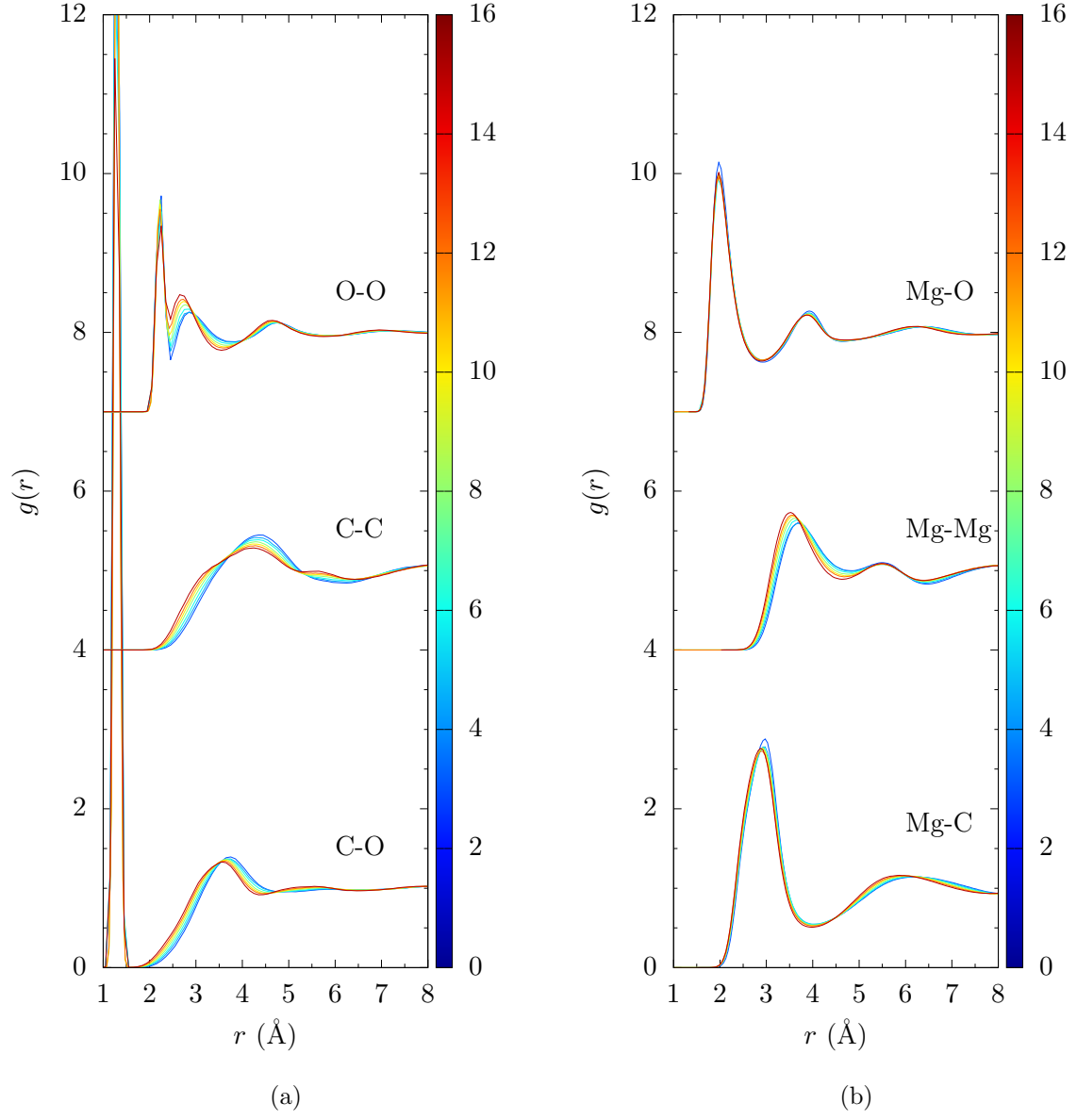


FIG. S1. Pressure evolution of MD pair distribution functions in MgCO_3 at 2073 K (3 GPa) and at 2273 K (4.5, 6, 8, 10, 12 and 15 GPa). The color scale refers to the pressure (in GPa). To facilitate visualization, the different PDFs were shifted vertically.

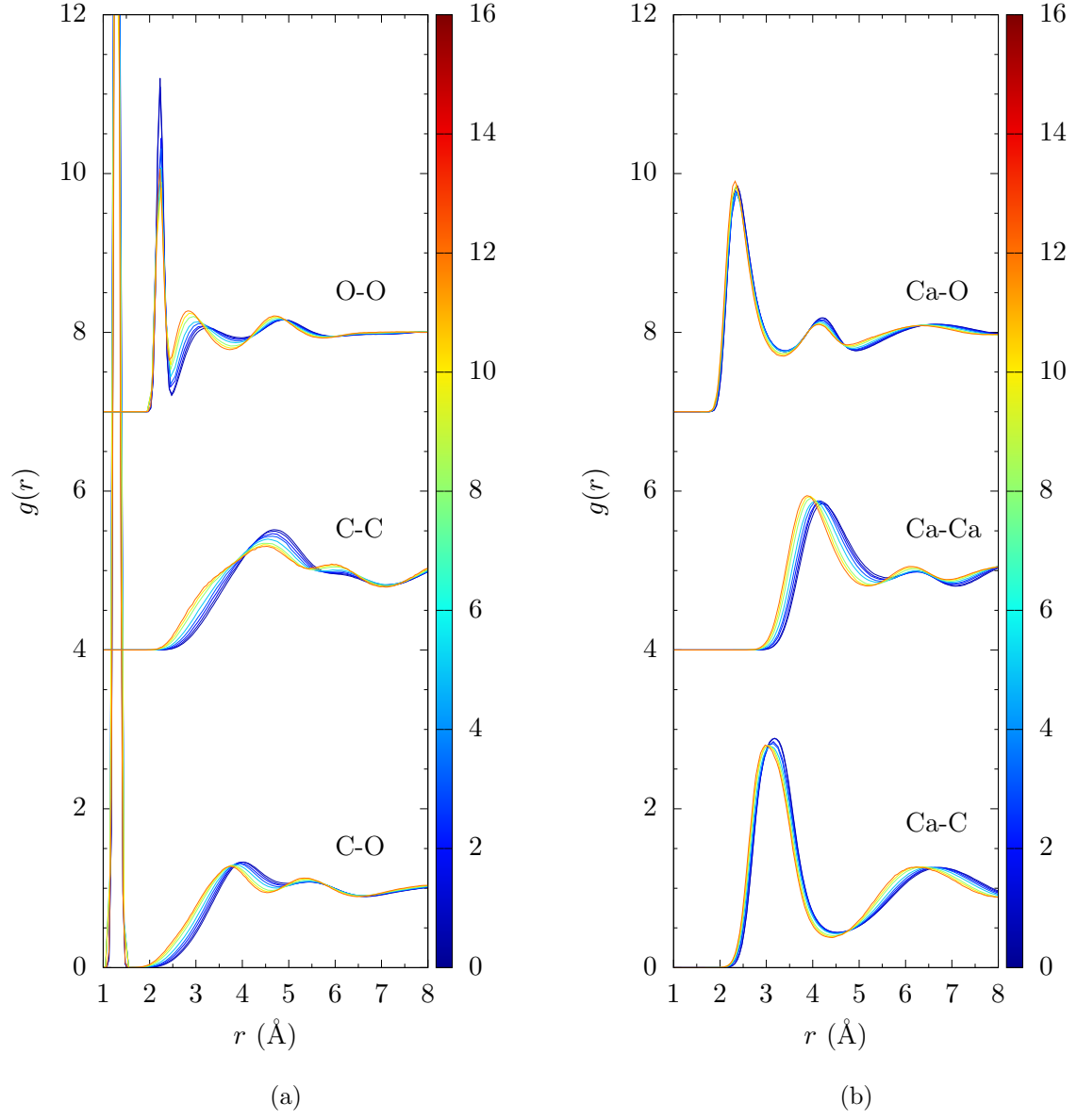


FIG. S2. Pressure evolution of MD pair distribution functions in **CaCO₃** at 1773 K (0.5 and 1 GPa), 1923 K (2 and 3 GPa) and 2073 K (5, 8, 10 and 12 GPa). The color scale refers to the pressure (in GPa). To facilitate visualization, the different PDFs were shifted vertically.

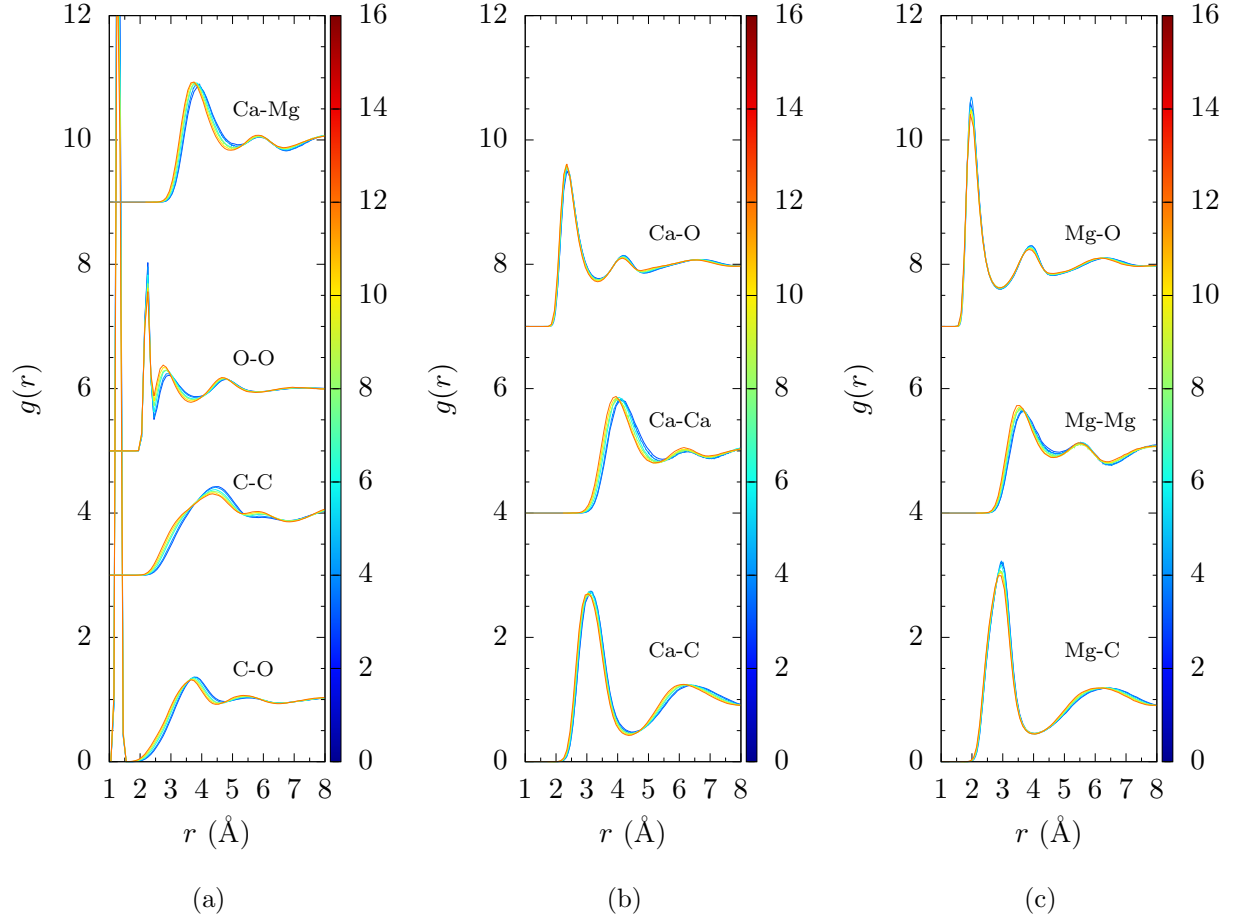


FIG. S3. Pressure evolution of MD pair distribution functions in $\text{CaMg}(\text{CO}_3)_2$ at 1873 K (3, 4 and 6 GPa) and 2073 K (8, 10 and 12 GPa). The color scale refers to the pressure (in GPa). To facilitate visualization, the different PDFs were shifted vertically.

	T (K)	$\langle T \rangle$ (K)	n (g/cm ³)	$\langle P \rangle$ (kbar)	σ (S/m)	η (mPa·s)	D_{Mg} (10 ⁻⁹ m ² /s)	D_{CO_3} (10 ⁻⁹ m ² /s)
<hr/>								
MgCO ₃								
	1940	1897	2.49	20	298 ± 5	5.3 ± 0.2	2.89	1.98
	1940	1943	2.49	22	323 ± 5	5.1 ± 0.2	3.11	2.13
AIMD	1873	1936	2.49	45 ± 15	/	/	4.4 ± 0.5	3.2 ± 0.5
	1823	1815	2.60	31	240 ± 10	7.0 ± 0.3	2.10	1.41
	1923	1926	2.56	30	285 ± 15	5.7 ± 0.5	2.70	1.83
	2073	2041	2.53	29	330 ± 5	4.9 ± 0.3	3.35	2.25
	1873	1868	2.61	35	258 ± 10	6.9 ± 0.3	2.24	1.53
	1873	1840	2.68	44	225 ± 10	8.1 ± 0.3	1.85	1.30
	2073	2039	2.64	44	285 ± 15	5.8 ± 0.2	2.8	1.92
	2273	2265	2.60	45	373 ± 10	4.6 ± 0.2	4.02	2.75
	2073	2098	2.73	61	275 ± 5	6.7 ± 0.5	2.55	1.80
	2173	2183	2.71	60	315 ± 10	5.7 ± 0.6	3.05	2.12
	2273	2250	2.69	59	335 ± 20	5.3 ± 0.4	3.30	2.37
	2073	2046	2.83	79	210 ± 5	8.2 ± 0.2	1.90	1.35
	2273	2276	2.79	80	290 ± 10	6.2 ± 0.3	2.95	2.20
	2273	2280	2.88	100	235 ± 10	8.0 ± 0.3	2.40	1.75
	2273	2264	2.96	120	215 ± 15	8.8 ± 0.5	2.00	1.45
	2273	2261	3.06	149	174 ± 5	11.5 ± 0.5	1.55	1.18
<hr/>								

TABLE S3. Thermodynamic averages and transport coefficients issued from all MD simulations of **MgCO₃**. Diffusion coefficients estimated from the AIMD simulations are also mentioned (AIMD).

	T (K)	$\langle T \rangle$ (K)	n (g/cm ³)	$\langle P \rangle$ (kbar)	σ (S/m)	η (mPa·s)	D_{Ca} (10 ⁻⁹ m ² /s)	D_{CO_3} (10 ⁻⁹ m ² /s)
<hr/>								
CaCO ₃								
	1623	1622	2.33	4.9	210 ± 15	5.3 ± 0.3	1.95	1.82
AIMD (Ref. S6)	1623		2.30	5 ± 5	171 ± 15	5.3 ± 0.5	2.4 ± 0.2	1.6 ± 0.2
	1773	1772	2.28	5.0	235 ± 20	4.1 ± 0.3	2.75	2.45
	2073	2057	2.20	4.9	335 ± 10	2.9 ± 0.3	4.75	4.05
	1653	1640	2.37	8.7	/	6.0 ± 0.3	/	/
	1653	1648	2.37	8.8	195 ± 10	5.8 ± 0.2	1.84	1.74
	1773	1773	2.35	10	220 ± 20	4.9 ± 0.3	2.38	2.18
	2073	2046	2.27	9.5	330 ± 10	3.4 ± 0.3	4.00	3.65
	1923	1906	2.42	20	236 ± 10	5.9 ± 0.4	2.50	2.37
	1813	1796	2.52	28	170 ± 10	7.2 ± 0.5	1.63	1.60
	1923	1919	2.51	30	210 ± 10	5.6 ± 0.5	2.03	2.02
	2073	2058	2.48	30	230 ± 10	5.0 ± 0.5	2.70	2.56
	1773	1771	2.66	45	120 ± 10	10.5 ± 0.5	1.05	1.11
AIMD (Ref. S6)	1773		2.64	45 ± 5	147 ± 15	10.5 ± 2.0	1.2 ± 0.2	1.0 ± 0.2
	1923	1913	2.63	45	156 ± 10	8.2 ± 0.3	1.57	1.57
	2073	2063	2.63	50	180 ± 10	6.8 ± 0.3	2.00	2.00
	2063	2041	2.70	61	155 ± 5	8.1 ± 0.2	1.57	1.59
	2063	2060	2.70	62	/	7.9 ± 0.3	/	/
	2073	2056	2.80	79	117 ± 5	9.7 ± 0.9	1.29	1.24
	2073	2040	2.90	99	90 ± 5	13.8 ± 0.4	0.93	0.96
	2073	2064	2.98	122	71 ± 5	16.3 ± 0.9	0.79	0.85
AIMD (Ref. S6)	2073		2.94	122 ± 10	102 ± 20	12.4 ± 2.5	1.2 ± 0.2	1.1 ± 0.2
<hr/>								

TABLE S4. Thermodynamic averages and transport coefficients issued from all MD simulations of **CaCO₃**. Diffusion coefficients estimated from the AIMD simulations are also mentioned (AIMD Ref. S6).

	T (K)	$\langle T \rangle$ (K)	n (g/cm ³)	$\langle P \rangle$ (kbar)	σ (S/m)	η (mPa·s)	D_{Mg} (10 ⁻⁹ m ² /s)	D_{Ca} (10 ⁻⁹ m ² /s)	D_{CO_3} (10 ⁻⁹ m ² /s)
<hr/>									
CaMg(CO ₃) ₂	1773	1755	2.25	1	272 ± 5	4.1 ± 0.3	2.93	3.0	2.39
AIMD	1773		2.25	18 ± 10	140 ± 50		5.5 ± 0.3	5.0 ± 0.3	3.9 ± 0.5
	1773	1775	2.49	20	201 ± 10	6.3 ± 0.3	2.08	1.90	1.66
	1573	1571	2.62	30	112 ± 10	12 ± 0.5	0.91	0.80	0.77
	1683	1700	2.59	30	158 ± 10		1.37	1.20	1.12
	1683	1679	2.59	30	/	9.6 ± 1	/	/	/
	1873	1859	2.55	31	195 ± 15	6.9 ± 1	2.05	1.80	1.63
	2073	2065	2.51	30	275 ± 10	4.8 ± 0.5	3.15	2.80	2.47
	1653	1650	2.64	35	123 ± 10	11.7 ± 0.6	1.08	0.92	0.89
	1653	1685	2.67	41	118 ± 5	11.4 ± 0.2	1.06	0.92	0.91
	1873	1850	2.63	39	173 ± 10	7.9 ± 0.2	1.65	1.47	1.40
	1653	1659	2.71	45	103 ± 5	13.2 ± 0.3	0.90	0.78	0.76
	1653	1627	2.74	49	92 ± 3	16.5 ± 0.5	0.73	0.62	0.62
	1783	1782	2.73	53	125 ± 5	11.1 ± 0.5	1.13	0.98	0.96
	1623	1604	2.80	59	72 ± 7	22.5 ± 1.5	0.55	0.47	0.48
	1873	1878	2.75	60	130 ± 5	10.7 ± 0.5	1.33	1.15	1.11
	2073	2078	2.71	60	188 ± 10	7.5 ± 0.5	2.10	1.85	1.73
	2073	2060	2.85	79	150 ± 10	9.3 ± 0.2	1.60	1.34	1.30
	2073	2054	2.91	99	118 ± 5	12.1 ± 0.5	1.25	1.05	1.05
	2073	2067	2.99	120	83 ± 10	16.9 ± 0.5	1.02	0.85	0.85
<hr/>									

TABLE S5. Thermodynamic averages and transport coefficients issued from all MD simulations of **CaMg(CO₃)₂**. Diffusion coefficients estimated from the AIMD simulations are also mentioned (AIMD).

	T	$\langle T \rangle$	n	$\langle P \rangle$	σ	η	D_{X_1}	D_{X_2}	D_{CO_3}
	(K)	(K)	(g/cm ³)	(kbar)	(S/m)	(mPa·s)	(10 ⁻⁹ m ² /s)	(10 ⁻⁹ m ² /s)	(10 ⁻⁹ m ² /s)
<hr/>									
Na ₂ CO ₃ -MgCO ₃									
0.50:0.50 (mol)	1323	1321	2.45	0.3-0.7	30	98 ± 5	15.3 ± 1	1.52	0.56
	1573	1576	2.40		29	186 ± 10	6.9 ± 0.2	3.80	1.48
<hr/>									
K ₂ CO ₃ -MgCO ₃									
0.75:0.25 (mol)	1573	1580	2.33		30	105 ± 5	6.7 ± 0.5	3.06	1.10
0.50:0.50 (mol)	1273	1247	2.48		29	20 ± 3	60 ± 7	0.42	0.13
	1373	1367	2.45		30	38 ± 5	26.3 ± 1	0.87	0.32
	1473	1468	2.42		30	58 ± 5	16.5 ± 1	1.39	0.53
	1573	1561	2.40		30	75 ± 10	11.7 ± 0.5	1.98	0.81
	1673	1687	2.37		30	102 ± 5	7.7 ± 0.6	2.80	1.24
0.56:0.44 (mol)	1673	1645	2.39		29	94 ± 5	9.6 ± 0.3	2.28	1.06
0.25: 0.75 (mol)	1673	1654	2.47		29	102 ± 5	11.2 ± 0.2	1.70	1.06
<hr/>									
K ₂ CO ₃ -CaCO ₃									
0.50:0.50 (mol)	1100	1094	2.14		0	70 ± 5	15.1 ± 1.5	1.38	0.45
	1200	1189	2.09		0	100 ± 10	9.0 ± 0.5	2.15	0.74
	1223	1211	2.44		25	30 ± 1	35 ± 5	0.61	0.24
	1423	1403	2.38		24	75 ± 10	12	1.64	0.68
	1300	1288	2.46		30	37 ± 5	28 ± 5	0.77	0.31
	1573	1584	2.39		30	95 ± 10	9 ± 0.5	2.45	1.12
<hr/>									

TABLE S6. Thermodynamic averages and transport coefficients issued from all MD simulations of binary mixtures **Na₂CO₃-MgCO₃**, **K₂CO₃-MgCO₃** and **K₂CO₃-CaCO₃**. The notation X₁ (= Na or K) and X₂ (= Mg or Ca) are assigned in the same order as appearing in the composition name (first column).

	T (K)	$\langle T \rangle$ (K)	n (g/cm ³)	$\langle P \rangle$ (kbar)	σ (S/m)	η (mPa·s)	D_{X_1} (10 ⁻⁹ m ² /s)	D_{X_2} (10 ⁻⁹ m ² /s)	D_{Ca} (10 ⁻⁹ m ² /s)	D_{CO_3}
<hr/>										
LiCO ₃ -NaCO ₃ -CaCO ₃										
0.21:0.49:0.30 (mol)	900	904	2.18	0	70 ± 5	25 ± 3	0.98	0.78	0.28	0.24
	1000	1000	2.13	0	120 ± 5	11.8 ± 1	1.80	1.42	0.54	0.48
<hr/>										
NaCO ₃ -K ₂ CO ₃ -CaCO ₃										
0.55:0.09:0.36 (mol)	823	832	2.27	0	24.5 ± 1	68 ± 10	0.27	0.20	0.07	0.06
(natrocarbonatite)	1073	1070	2.14	0	105 ± 5	10.5 ± 0.5	1.74	1.43	0.61	0.54
<hr/>										
0.25:0.25:0.50 (mol)										
	1000	1005	2.21	0	52 ± 5	35 ± 10	0.90	0.73	0.27	0.24
	1100	1105	2.16	0	82 ± 10	15.2 ± 1	1.27	1.50	0.50	0.45
<hr/>										

TABLE S7. Thermodynamic averages and transport coefficients issued from all MD simulations of ternary mixtures **Li₂CO₃-Na₂CO₃-CaCO₃** and **Na₂CO₃-K₂CO₃-CaCO₃**. The notation X₁ (= Li or Na) and X₂ (= Na or K) are assigned in the same order as appearing in the composition name (first column).

REFERENCES

- [S1]S. A. Markgraf and R. J. Reeder, [Am. Mineral. **70**, 590 \(1985\)](#).
- [S2]S. A. T. Redfern, B. J. Wood, and C. M. B. Henderson, [Geophys. Res. Lett. **20**, 2099 \(1993\)](#).
- [S3]G. Fiquet, F. Guyot, and J.-P. Itie, [Am. Mineral. **79**, 15 \(1994\)](#).
- [S4]J. Zhang, I. Martinez, F. Guyot, P. Gillet, and S. K. Saxena, [Phys. Chem. Miner. **24**, 122 \(1997\)](#).
- [S5]N. L. Ross, [Am. Mineral. **82**, 682 \(1997\)](#).
- [S6]R. Vuilleumier, A. Seitsonen, N. Sator, and B. Guillot, [GCA **141**, 547 \(2014\)](#).